



www.asianpubs.org

ARTICLE

## Quantum Computational, Spectroscopic and Molecular Docking Studies on *N*-(4-Hydroxyphenyl)picolinamide

Meenakshi Singh<sup>1</sup>, Mukesh Kumar<sup>1,2</sup>, Neha Singh<sup>1</sup>, Shikha Sharma<sup>1</sup>, Neha Agarwal<sup>1</sup>, Indresh Verma<sup>3</sup>, Satyavir Singh<sup>2</sup>, Nazia Siddiqui<sup>4,✉</sup> and Saleem Javed<sup>1,✉</sup>

### ABSTRACT

In this work, the quantum computations of newly synthesized *N*-(4-hydroxyphenyl)picolinamide (4-HPP) is focused. Density functional theory (DFT) was used to perform the quantum calculations. The optimized molecular geometry was obtained using the B3LYP and MP2 methods employing 6-311++G(d,p) basis set, which served as the foundation for all subsequent calculations. The experimental data was compared with the calculated vibrational frequencies and NMR spectra. With the use of the molecular electrostatic potential surface (MEP) and the Fukui functions, the charge distribution, reactive regions and electrostatic potential were displayed. The chemical activity of the 4-HPP was evaluated by the energy difference between HOMO and LUMO. For better understanding of the intermolecular charge transfer (ICT), natural bond order analysis (NBO) was used. At various temperatures, thermodynamic parameters such as Gibb's free energy, enthalpy and entropy were determined. The electrophilicity index was used to portray the molecule's bioactivity and molecular docking was used to show the interaction between the ligand and the protein. The nature of the molecule was determined by drug similarity when expecting its application for medical purposes.

### KEYWORDS

Picolinamide, Quantum computation, Fukui functions, Natural bond order analysis, Molecular docking, Drug-likeness.

### INTRODUCTION

The amide linkage (-CO-NH-) is a distinct structural unit in the protein skeleton. These are thought to be suitable for drug research due to their biological compatibility. Fungicidal [1-4], herbicidal [5-10], anticancer [11,12] activities, *etc.* are among the many applications/properties of amide derivatives [13]. The anti-inflammatory, analgesic and antipyretic properties of pyridinecarboxamide derivatives have been reported [14]. Many diamide derivatives show significant larvicidal action against the *Culex* mosquito, which transmits diseases such as filariasis, West Nile fever, dengue fever, chikungunya, yellow fever and encephalitis [15].

*N,N*-Dipyridyl-2,6-pyridinedicarboxamide has been claimed to alleviate atherosclerosis in some studies [14]. Anti-cancer and antibacterial activity is notable in coordination

## Asian Journal of Organic & Medicinal Chemistry

Volume: 6                      Year: 2021  
Issue: 3                        Month: July–September  
pp: 186-203  
DOI: <https://doi.org/10.14233/ajomc.2021.AJOMC-P334>

Received: 2 August 2021  
Accepted: 1 September 2021  
Published: 30 September 2021

#### Author affiliations:

<sup>1</sup>Department of Chemistry, Institute of Home Science, Khandari, Dr. Bhimrao Ambedkar University, Agra-282002, India

<sup>2</sup>Department of Chemistry, Shri Khushal Das University, Hanumangarh-335801, India

<sup>3</sup>Department of Chemistry, Indian Institute of Technology, Kanpur-208016, India

<sup>4</sup>USIC, Dayal Bagh Educational Institute, Agra-282005, India

✉To whom correspondence to be addressed:

E-mail: [dr.naazsiddiqui@gmail.com](mailto:dr.naazsiddiqui@gmail.com); [saleem.7javed@gmail.com](mailto:saleem.7javed@gmail.com)

Available online at: <http://ajomc.asianpubs.org>

complexes of various amide-based drugs with minor adverse effects [16-19].

Because of their antioxidant and biological activities, phenol and catechol-based compounds are a topic of interest. Phenol (or catechol) takes on rigid conformations that promote the activation of immune-competent cells, which boosts immunity and has antitumor properties [20]. Only a few catechol groups are known to have anesthetic and analgesic properties and their activity shrinks the molecule [21].

As shown in the synthetic systems, the presence of several hydroxyl groups in a molecule is thought to increase their affinity for protein and nucleic acid due to the existence of hydrogen bond providers and acceptors [22-31]. Despite the importance of amide and phenol/catechol groups in a variety of applications, hybrid molecules are rarely studied. This article reports a DFT investigation of *N*-(4-hydroxy-phenyl)picolinamide (4-HPP), in which several essential features of the molecule, as well as molecular docking and drug-likeness, are also investigated.

## EXPERIMENTAL

All experimental details and comparison data are drawn from the published data [32,33].

**Computational details:** The quantum calculation on the *N*-(4-hydroxyphenyl)picolinamide (4-HPP) molecule was performed with the Gaussian 03 W program [34] and Orca 4.0.1 [35] software, utilizing the B3LYP method and 6311++G(d,p) basis set. The DFT and MP2 methods were used to optimize the molecular geometry using the 6311++G(d,p) basis set. Further calculations such as the HOMO-LUMO energy gap and the molecular electrostatic potential (MEP) were performed using the optimized geometry from DFT. The computed wavenumber's potential energy distribution (PED) was determined using the VEDA4 program [36]. Multiwfn was used to calculate the electron localization function (ELF) as well as to display the IR and Raman spectra [37]. Molecular docking was performed using the Autodock-Vina and Chimera software [38,39]. The drug's characteristics were determined using the SwissADME tool [40]. The ionization potential (IP) and electron affinity (EA) were calculated using Koopman's theorem, *i.e.*,  $EA = -E_{\text{HOMO}}$  and  $IP = -E_{\text{LUMO}}$  [41]. The chemical reactivity descriptors can be created by applying the following equations to IP and EA:

$$\text{Electronegativity } (\chi) = \frac{IA + EA}{2}$$

$$\text{Chemical potential } (\mu) = -\frac{(IA + EA)}{2}$$

$$\text{Chemical hardness } (\eta) = -\frac{IA - EA}{2}$$

$$\text{Chemical softness } (\sigma) = \frac{1}{2\eta}$$

$$\text{Electrophilicity index } (\omega) = \mu \times \frac{\mu}{2\eta}$$

## RESULTS AND DISCUSSION

**Geometry optimization:** The B3LYP/6311++G(d,p) method and basis set were used to optimize the geometry of the molecule. The *N*-(4-hydroxyphenyl)picolinamide (4-HPP) molecule possess C1 point group and the geometric properties of the named molecule are listed in Table-1. The N-H bond length calculated by DFT method is in the range of 1.33-1.40 Å while for experimental, it is between 1.34- 1.43 Å; for N-O, DFT calculated bond length is 1.23 Å and the experimental bond length is 1.24 Å. The RMSD value between the experimental and calculated value for bond lengths is 0.984 and R<sup>2</sup> value is 0.969. Similarly, the DFT calculated bond angle of N-O-C is 126.035° and the experimentally calculated bond angle is 120.304. The optimize structure with numbering is shown in Fig. 1.

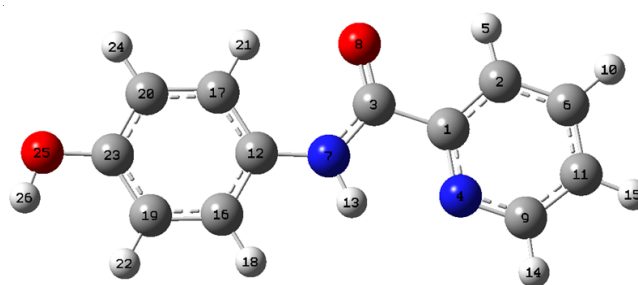


Fig. 1. Optimized labelled structure of 4-HPP

**Vibrational analysis:** The significant vibrational observations of the studied molecule were compared to DFT-calculated spectra using 6311++G. (d,p). To reduce the difference between experimental and theoretical values, a small scaling factor of 0.961 was utilized. This is because of the presence of solid and gas forms when calculated experimentally and theoretically, respectively. The variance is less than 10 cm<sup>-1</sup> after scaling.

The C1 point group is represented by 29 atoms of the molecule and 72 fundamental vibrational modes. The molecule is at the lowest point on the potential energy surface if there are no imaginary frequency values. The VEDA program estimated partial energy distribution (PED assignment) to characterize vibrational modes. Table-2 lists the IR and Raman activities and Fig. 2a and 2b show the related graphs (b).

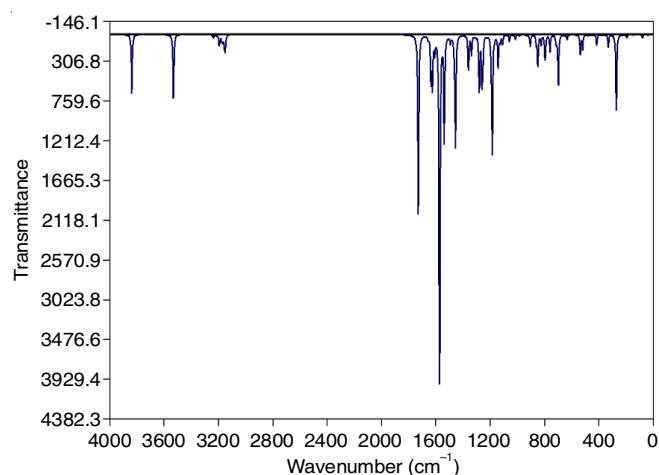


Fig. 2(a). FT-IR spectra of 4-HPP using b3LYP/6311++G(d,p)

TABLE-1  
OPTIMIZED GEOMETRICAL PARAMETERS OF 4-HPP: BOND LENGTH (Å) AND BOND ANGLES (°)

Bond length (Å)			Bond angle (°)				
Parameter	B3LYP/6-311++G(d,p)	MP2/6-311++G(d,p)	Experimental	Parameter	B3LYP/6-311++G(d,p)	MP2/6-311++G(d,p)	Experimental
C1-C2	1.3948	1.4004	1.3694	C2-C1-C3	118.9606	118.7208	121.152
C1-C3	1.5146	1.5116	1.4814	C2-C1-C4	123.0703	123.5708	121.891
C1-N4	1.3399	1.3476	1.3444	C3-C1-C4	117.9692	117.7084	116.957
C2-H5	1.0819	1.0848	0.9289	C1-C2-H5	119.0504	119.0899	119.727
C2-C6	1.3906	1.3957	1.3688	C1-C2-C6	118.3181	118.3047	120.395
C3-N7	1.3613	1.3626	1.3235	H5-C2-C6	122.6315	122.6054	119.877
C3-O8	1.2239	1.2289	1.2434	C1-C3-O8	121.0534	121.2376	120.432
N4-C9	1.3341	1.3430	1.3527	N7-C3-O8	026.0351	126.3208	120.304
C6-H10	1.0841	1.0865	0.9300	C1-N4-C9	118.1563	117.3972	117.294
C6-C11	1.3926	1.3988	1.3744	C2-C6-H10	120.462	120.6014	121.107
N7-C12	1.4088	1.4063	1.4349	C2-C6-C11	118.9395	118.7583	117.662
N7-H13	1.0146	1.0166	0.7576	C1-C3-O8	121.0534	121.2376	120.432
O8-H21	2.2462	2.2470	2.2802	H10-C6-C11	120.5989	120.6402	121.271
C9-C11	1.3941	1.3991	1.3522	C3-N7-C12	129.2628	128.6881	131.316
C9-H14	1.0859	1.0878	0.9294	C3-N7-H13	113.2902	113.4084	103.337
C11-H15	1.0833	1.0858	0.9296	C12-N7-H13	117.447	117.9035	124.952
C12-C16	1.3998	1.4046	1.4128	N4-C9-C11	1123.0234	123.3655	122.647
C12-C17	1.4026	1.4067	1.3569	N4-C9-H14	116.2933	115.994	118.728
C16-H18	1.0853	1.0881	0.9308	C11-C9-H14	120.6833	120.6405	118.625
C16-C19	1.3903	1.3964	1.3573	C6-C11-C9	118.4924	118.6035	120.141
C17-C20	1.3901	1.3969	1.3967	C6-C11-H15	121.3559	121.332	119.967
C17-H21	1.0794	1.0818	0.9303	C9-C11-H15	120.1517	120.0644	119.892
C19-H22	1.0859	1.0885	0.9316	N7-C12-C16	117.6085	117.2931	119.906
C19-C23	1.3951	1.4001	1.3791	N7-C12-C17	123.497	123.4754	121.887
C20-C23	1.3938	1.398	1.3494	C16-C12-C17	118.8945	119.2316	118.202
C20-H24	1.0833	1.0861	0.9297	C12-C16-H18	119.7846	119.7382	119.750
C23-O25	1.3716	1.3718	1.4056	C12-C16-C19	120.8764	120.7251	120.589
O25-H26	0.9625	0.9624	0.8022	H18-C16-C19	119.339	119.5367	119.661
				C12-C17-C20	120.0396	119.7157	120.773
				C12-C17-H21	119.4952	119.8398	119.565
				C20-C17-H21	120.4652	120.4445	119.662
				C16-C19-H22	119.7008	119.709	120.034
				C16-C19-C23	119.9541	119.9159	120.036
				H22-C19-C23	120.3451	120.3752	119.929
				C17-C20-C23	120.7649	120.9004	120.025
				C17-C20-H24	120.3009	120.2415	120.026
				C23-C20-H24	118.9342	118.8581	119.948
				C19-C23-C20	119.4705	119.5113	120.322
				C19-C23-O25	122.8379	122.9765	120.734
				C20-C23-O25	117.6916	117.5122	118.938
				C23-O25-H26	109.7752	108.4378	100.995

TABLE-2  
CALCULATED VIBRATIONAL FREQUENCIES (cm<sup>-1</sup>) ASSIGNMENTS OF 4-HPP BASED ON B3LYP/6-311++G(d,p) BASIS SET

Mode No.	Experimental wavenumber (cm <sup>-1</sup> )	Theoretical wavenumber (cm <sup>-1</sup> )		I <sub>IR</sub> <sup>c</sup>	I <sub>RAMAN</sub> <sup>d</sup>	Assignments (PED) <sup>(a,b)</sup>
	FT-IR	Unscaled	Scaled			
72	3299	3464	3328	20	16	γNH(100)
71	3244	3388	3256	7	46	γOH(88)
70	–	3314	3185	3	30	γCH(77)
69	–	3314	3185	8	8	γCH(43)
68	–	3310	3181	3	15	γCH(88)
67	–	3304	3175	3	18	γCH(65)
66	–	3297	3168	51	22	γCH(57)
65	–	3292	3164	1	5	γCH(72)
64	–	3291	3163	0	8	γCH(86)
63	–	1764	1695	0	9	γCH(18)
62	–	1758	1689	4	29	γCC(41) + βCNC(10)
61	1668	1727	1660	9	20	γCC(42) + γNC(11) + γOC(28)
60	1602	1675	1609	12	30	CC(46) + γNC(27)

59	-	1597	1535	100	12	$\gamma\text{CC}(13) + \gamma\text{CN}(21) + \beta\text{HNC}(44) +$
58	-	1572	1511	99	100	$\gamma\text{CC}(13) + \beta\text{HCC}(41)$
57	-	1544	1484	23	6	$\beta\text{HCC}(18) + \beta\text{HCN}(10) + \beta\text{CCN}(12)$
56	-	1516	1457	62	6	$\gamma\text{OC}(26) + \beta\text{HNC}(30)$
55	-	1490	1432	5	15	$\gamma\text{CC}(19) + \gamma\text{NC}(19) + \beta\text{HNC}(22) + \beta\text{HCC}(19)$
54	-	1471	1414	27	41	$\gamma\text{CC}(43)$
53	-	1452	1395	41	3	$\beta\text{HCC}(19) + \beta\text{CCC}(11)$
52	-	1374	1320	3	4	$\gamma\text{NC}(57) + \beta\text{HCC}(11)$
51	-	1336	1284	9	2	$\beta\text{HCC}(73)$
50	-	1286	1236	0	4	$\gamma\text{NC}(18) + \beta\text{HCC}(16) + \beta\text{HCN}(36)$
49	-	1244	1195	4	41	$\gamma\text{CC}(15) + \beta\text{HNC}(25)$
48	-	1229	1181	0	6	$\gamma\text{CC}(19) + \gamma\text{OC}(10) + \beta\text{HCC}(23)$
47	-	1192	1146	0	0	$\beta\text{HOC}(23) + \beta\text{HCC}(31)$
46	-	1190	1144	1	2	$\beta\text{HOC}(19) + \beta\text{HCC}(35)$
45	-	1170	1124	1	3	$\gamma\text{NC}(10) + \beta\text{HNC}(11) + \beta\text{HCC}(14)$
44	-	1162	1117	55	20	$\gamma\text{CC}(21) + \beta\text{HOC}(31) + \beta\text{HCC}(14)$
43	-	1150	1105	3	13	$\gamma\text{CC}(10) + \beta\text{HCC}(44)$
42	-	1138	1094	33	11	$\gamma\text{NC}(12) + \beta\text{HCC}(19) + \beta\text{CCC}(11)$
41	-	1130	1086	2	14	$\gamma\text{NC}(16) + \beta\text{CCC}(13) + \beta\text{CNC}(15)$
40	-	1113	1070	5	0	$\gamma\text{CC}(17) + \beta\text{HCC}(18) + \beta\text{HCN}(10)$
39	-	1044	1003	18	0	$\gamma\text{CC}(20) + \beta\text{CCC}(23) + \beta\text{HCC}(16)$
38	-	1036	996	8	4	$\gamma\text{NC}(19) + \beta\text{CNC}(24)$
37	-	999	960	0	0	$\tau\text{HCCC}(52)$
36	-	979	941	1	0	$\tau\text{HCCC}(48) + \tau\text{CNCC}(12)$
35	-	950	913	0	0	$\tau\text{HCCC}(51)$
34	-	912	876	11	1	$\beta\text{OCN}(39) + \beta\text{CNC}(11)$
33	-	884	850	0	0	$\tau\text{HCCC}(28)$
32	-	879	845	0	0	$\tau\text{HCCC}(26)$
31	-	850	817	1	6	$\gamma\text{CC}(24) + \gamma\text{NC}(12) + \gamma\text{OC}(25)$
30	-	829	797	8	0	$\tau\text{HCCC}(12)$
29	-	815	783	8	0	$\tau\text{HCCC}(30)$
28	-	767	737	21	1	$\gamma\text{NC}(16) + \gamma\text{OC}(18) + \gamma\text{CC}(10) + \beta\text{CCC}(10)$
27	-	746	717	7	0	$\tau\text{HCCC}(72)$
26	-	718	690	1	0	$\tau\text{HCCC}(18) + \tau\text{CNCC}(45)$
25	-	699	672	6	0	$\tau\text{HCCC}(15)$
24	-	693	666	0	1	$\gamma\text{NC}(10) + \gamma\text{OC}(11) + \beta\text{CCC}(10) + \beta\text{OCN}(10) + \beta\text{CCN}(12)$
23	-	680	653	11	0	$\tau\text{HCCC}(12)$
22	-	671	645	1	1	$\beta\text{CCC}(26)$
21	-	635	610	2	1	$\beta\text{CCC}(26) + \beta\text{CNC}(28)$
20	-	533	512	8	1	$\beta\text{CCC}(16) + \beta\text{NCC}(16) + \beta\text{CNC}(14)$
19	-	488	469	37	0	$\tau\text{HNCC}(34) + \tau\text{HCCC}(17) + \tau\text{CNCC}(11)$
18	-	481	462	1	0	$\gamma\text{CC}(12) + \beta\text{CCC}(15)$
17	-	465	447	4	0	$\tau\text{HNCC}(51)$
16	-	459	441	3	0	$\tau\text{HCCC}(10) + \tau\text{CNCC}(19) + \tau\text{ONCC}(12)$
15	-	417	401	2	0	$\beta\text{OCC}(34) + \tau\text{CCCN}(11)$
14	-	412	396	3	0	$\beta\text{OCC}(23) + \tau\text{CCCN}(16)$
13	-	393	378	5	0	$\beta\text{OCN}(13) + \beta\text{CNC}(31) + \beta\text{CCN}(21)$
12	-	385	370	1	0	$\tau\text{CCCN}(11) + \tau\text{CCCC}(12)$
11	-	368	354	1	0	$\tau\text{CCC}(26) + \tau\text{CCCN}(10)$
10	-	333	320	1	0	$\beta\text{OCN}(33) + \beta\text{OCC}(11) + \beta\text{CCN}(10)$
9	-	357	343	0	0	$\tau\text{CCCN}(16) + \tau\text{CCCC}(12)$
8	-	271	260	0	0	$\gamma\text{NC}(18) + \gamma\text{CC}(10) + \beta\text{CNC}(15) + \beta\text{CCN}(18)$
7	-	254	244	0	0	$\gamma\text{NC}(16) + \gamma\text{CC}(23) + \beta\text{CCN}(16)$
6	-	210	201	0	0	$\gamma\text{CC}(12) + \beta\text{CCN}(27)$
5	-	198	190	0	0	$\tau\text{CCCC}(26) + \tau\text{CCCN}(15)$
4	-	144	138	0	0	$\gamma\text{CN}(21) + \beta\text{HCC}(10) + \tau\text{CNCC}(23)$
3	-	83	80	0	0	$\tau\text{CCCC}(13) + \beta\text{NCCC}(38)$
2	-	80	77	0	0	$\beta\text{CCN}(16) + \beta\text{NCC}(63)$
1	-	39	37	0	0	$\tau\text{CCCC}(27) + \tau\text{NCCC}(51)$

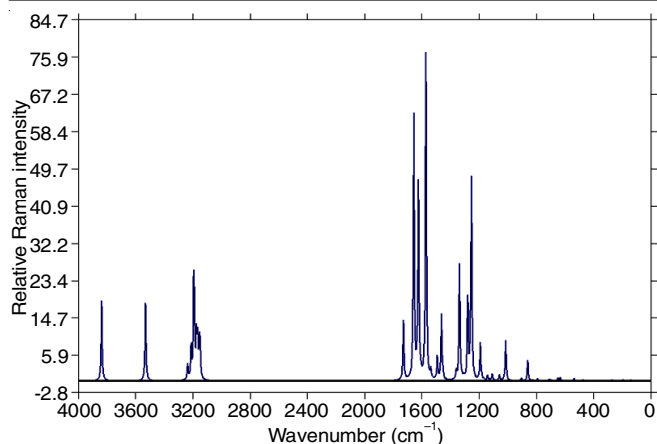


Fig. 2(b). FT-Raman spectra of 4-HPP using B3LYP/6311++G(d,p)

**N-H vibrations:** Usually the N-H stretching vibrations of heterocyclic compounds are observed in the region 3000–3500  $\text{cm}^{-1}$  [42]. 4-HPP has only one NH group observed at 3299  $\text{cm}^{-1}$  in FT-IR and the corresponding theoretically scaled wavenumber of 3328  $\text{cm}^{-1}$ , which is in good agreement with the reported wavenumber. It is a pure stretching mode with 100% contribution. Mixed vibrations due to stretching of C-C and C-N was observed at scaled wavenumber 1535 and 1432  $\text{cm}^{-1}$ .

**O-H vibrations:** The O-H group vibrations are very sensitive to the environment and show noticeable shifts in the spectra of hydrogen-bonded species. The hydroxyl stretching is generally observed near 3500  $\text{cm}^{-1}$ . The band due to the free hydroxyl group is sharp and has strong intensity. A broad band of less intensity is observed for solid, liquid and concentrated solutions [43,44]. In present study, stretching for O-H was observed at 3244  $\text{cm}^{-1}$  FT-IR spectra while the calculated wavenumber for the same is 3256  $\text{cm}^{-1}$  with a PED contribution of 88%.

**O-C vibrations:** The stretching of C=O group is normally expected in the 1740–1660  $\text{cm}^{-1}$  region [45,46]. Band assigned to -OH stretching at 1668  $\text{cm}^{-1}$  in the FT-IR spectra is quite close to calculated wavenumber 1660  $\text{cm}^{-1}$ . Mixed-mode stretching of OH bond was observed at calculated wavenumber 1457  $\text{cm}^{-1}$  while bending OH the HOC bond was calculated at 1146  $\text{cm}^{-1}$ .

**C-N vibrations:** It's a little difficult to recognize the C-N stretching in a side chain due to mixing. Pinchas *et al.* [47] assigned this stretching band at 1368  $\text{cm}^{-1}$  in benzamide. The frequency observed near 1500  $\text{cm}^{-1}$  corresponds to C=N bonds and the one closer to 1300  $\text{cm}^{-1}$  indicates the appearance of C-N bonds [48]. Stretching observed at 1602  $\text{cm}^{-1}$  and theoretically at 1609  $\text{cm}^{-1}$  exactly agrees with experimental observation.

Theoretically scaled wavenumbers at 1432  $\text{cm}^{-1}$  (mode no. 55), 1320  $\text{cm}^{-1}$  (mode no. 52), 1236  $\text{cm}^{-1}$  (mode no. 49), 1124  $\text{cm}^{-1}$  (mode no. 44), 1086  $\text{cm}^{-1}$  (mode no. 41), 996  $\text{cm}^{-1}$  (mode no. 38), 817  $\text{cm}^{-1}$  (mode no. 31), 737  $\text{cm}^{-1}$  (mode no. 28) with their PED contribution of 19, 57, 18, 10, 19, 12 and 16%, respectively.

**Molecular electrostatic potential surface (MEP):** This surface aids in the recognition of the molecule's electronic properties. This map depicts the variable charged region of a molecule in three dimensions, which is important for understanding the molecule's reactivity. The distinction between electrophilic and nucleophilic assaults is clarified.

The colour gradient is red to blue in the sequence of red, yellow, green and blue, with colour code values ranging from  $-5.593\text{e-}2$  (dark red) to  $5.593\text{e-}2$  (blue) (dark blue). The largest negative region due to the strongest repulsion is indicated by the red-coloured zone, which is a favourable site for electrophilic attack. The blue-coloured maximal positive zone indicates a place for nucleophilic attack due to the strongest attraction. The molecule's maximal sites are neutral, but the region above the oxygen atom (O8), an electronegative atom of the picolinamide ring, is red, as seen in Fig. 3. The most positive site identified by the blue-coloured region is the region near hydrogen (H26) of the hydroxyl group.

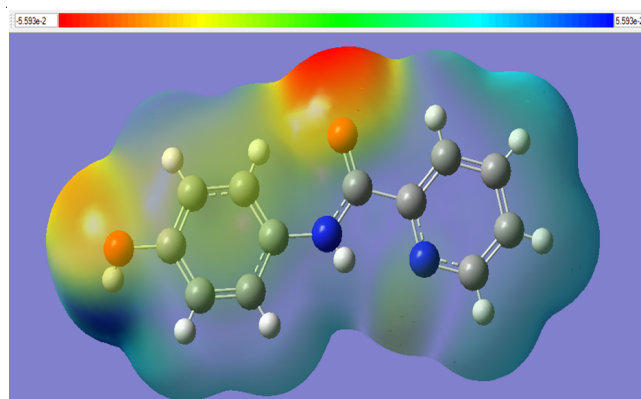


Fig. 3. Molecular electrostatic potential of 4-HPP

**Electron localization function (ELF):** The presence of localized electrons implies that discovering two electrons with opposite spins is a substantial possibility. ELF discusses a molecule's chemical structure, connectivity and reactivity. Fig. 4 shows an ELF colour-filled map. Because of the existence of well-localized electrons, the probability of detecting an electron or spin pair is highest at the region of maximum Pauli repulsion. It has the closest value to 1 and is coded in red. The region coded with a deep blue colour and a value of 0 is the space with the least Pauli repulsion and the lowest probability of discovering an electron spin pair due to the existence of delocalized electrons. The region around the H atom has the most Pauli repulsion, hence it appears red, whereas the region around the C atom is blue, indicating that it has the least Pauli repulsion.

**Non-linear optical properties (NLO):** The total molecular dipole moment ( $\mu_D$ ), linear polarizability ( $\alpha$ ) and first-order hyperpolarizability ( $\beta_{\text{tot}}$ ) were calculated on Gaussian 03W software for analyzing NLO properties using the DFT approach to show evidence of NLO character. Hyperpolarizability can fluctuate depending on the basis set used and the theoretical approach chosen [49–51]. This is the system's reaction to the applied electrical field. Because of hydrogen bond interactions, organic compounds with N-H groups are believed to have high hyperpolarizability and stability [52].

The highest dipole moment calculated by B3LYP/6311++G(d,p) was found to be on  $\mu_x = 2.6667$ . For the Y and Z axis, values were  $-3.7064$  and  $-0.0013$ , respectively (Table-3). The molecule has a higher contribution of  $\alpha_{xy}$ , which means that the molecule is polarized towards the X and Y direction. This high degree of polarizability reveals strong intermolecular interactions.

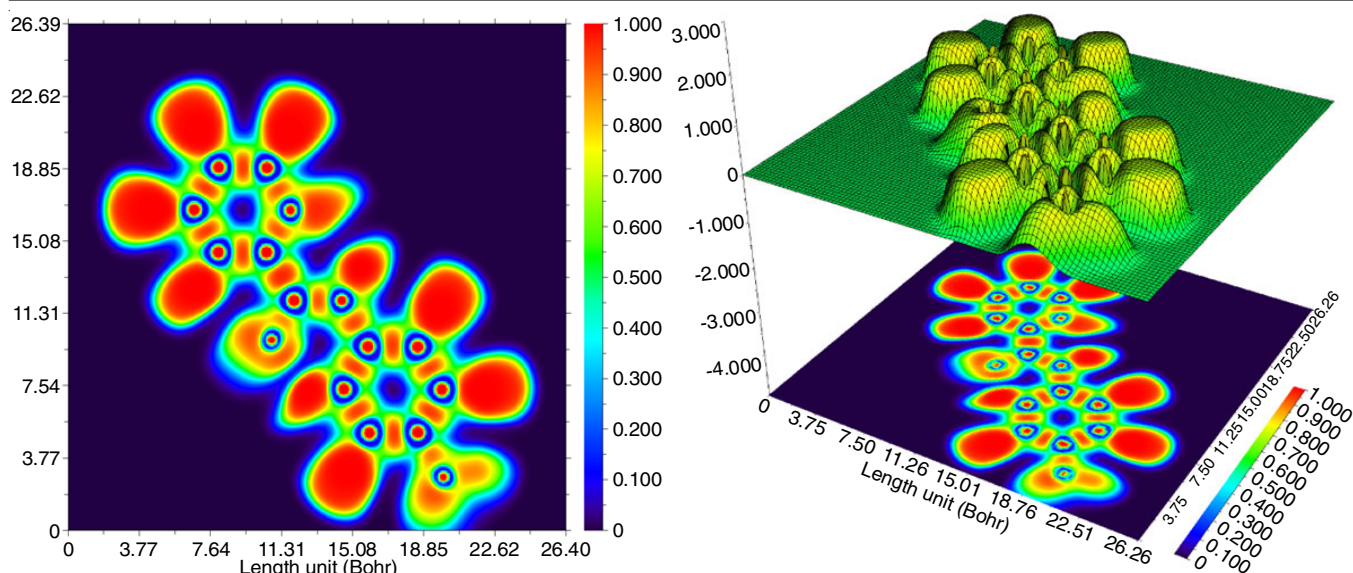


Fig. 4. ELF (colour filled and shaded surface map with projection) of hydrogen bond region in 4-HPP

TABLE-3  
VALUES OF CALCULATED DIPOLE MOMENT  
 $\mu$ (D), POLARIZABILITY ( $\alpha_0$ ), FIRST-ORDER  
HYPERPOLARIZABILITY, ( $\beta_{\text{tot}}$ ) COMPONENTS OF 4-HPP

Parameters	B3LYP/6-311++G(d,p)	Parameters	B3LYP/6-311++G(d,p)
$\mu_x$	2.6667	$\beta_{xxx}$	82.2421
$\mu_y$	-3.7064	$\beta_{yxx}$	-56.5735
$\mu_z$	-0.0013	$\beta_{xyy}$	-13.9908
$\mu$ (D)	4.5661	$\beta_{yyy}$	-16.5446
$\alpha_{xx}$	-68.1700	$\beta_{zxx}$	-0.1129
$\alpha_{xy}$	8.1668	$\beta_{xyz}$	-0.0565
$\alpha_{yy}$	-88.4739	$\beta_{zyy}$	0.0051
$\alpha_{zz}$	0.0103	$\beta_{xzz}$	-3.6246
$\alpha_{yz}$	0.0101	$\beta_{yzz}$	2.7703
$\alpha_{zz}$	-97.9135	$\beta_{zzz}$	-0.0036
$\alpha_0$ (e.s.u)	$-12.5751 \times 10^{-24}$	$\beta_{\text{tot}}$ (e.s.u)	$0.281 \times 10^{-30}$

**Natural bonding orbital (NBO) and natural hybrid orbitals (NHO) analysis:** The electron density transfer and hyperconjugative interaction between filled lone pair orbitals and unoccupied orbitals of the subsystems are interpreted using NBO analysis [53,54]. It's a quick and easy way to figure out intramolecular and intermolecular bonding, charge transfer and conjugative interactions [55,56]. NBO analysis has the advantage of being able to convey information on interactions between both filled and virtual orbitals, making it easier to investigate intramolecular and intermolecular interactions.

It depicts the various levels of donor-acceptors, bond types and occupancy levels in the compound. The degree of interaction between donors and acceptors is measured by stabilization energy ( $E_2$ ). The strength of interaction increases with the increase in  $E_2$  i.e., the more transfers from donors to acceptors, the higher the extent of conjugation [57]. The energy of stabilization is calculated as:

$$E^{(2)} = n_{\sigma} \frac{(F_{ij})^2}{\epsilon_{\sigma^*} - \epsilon_{\sigma}}$$

where  $E^{(2)}$  is associated with delocalization  $i \rightarrow j$ ,  $F_{ij}^2$  is the Fock matrix element between  $i$  and  $j$  orbitals.  $\epsilon_{\sigma}$  and  $\epsilon_{\sigma^*}$  are

energies of bonding and antibonding orbitals, respectively while  $n_{\sigma}$  is the population of  $\sigma$  orbitals.

In Table-4, the second-order perturbation analysis of the Fock matrix shows strong intramolecular hyperconjugative interactions. The donor-acceptor interaction present in the molecule is  $\pi(\text{C2-C6}) \rightarrow \pi^*(\text{C1-N4})$  and  $(\text{C9-N11})$  having energies 29.67 and 19.00 KJ/mol, respectively, they provide stability to the molecule. The stability of parts of the ring is due to the hyperconjugative interaction between  $\sigma$  and  $\pi$  electrons of C-C and antibonding C-C in the ring as indicated in Table-4. All these energies denote to  $(\text{C2-C6})$ ,  $(\text{C20-C23})$ ,  $(\text{C9-C11})$  and  $(\text{C16-C19})$ , which keeps occurring in backward and forward direction within the ring. Maximum occupancies obtained by  $\sigma(\text{C3-O8})$ ,  $\sigma(\text{C23-O25})$  and  $\sigma(\text{C3-C7})$  are 1.99395, 1.99260 and 1.98656, respectively. The result indicates that these orbitals are dominated by  $\pi$ -characters of hybrid orbitals.

The interaction energy related to resonance in a molecule is reckoned according to electron donation between  $\text{LP}(1)\text{N7} \rightarrow \pi^*(\text{C3-O8})$  and  $\pi^*(\text{C12-C17})$  having maximum stabilization energies 74.82 and 28.59 KJ/mol,  $\text{LP}(2)\text{O8} \rightarrow \pi^*(\text{C3-N7})$  and  $\pi^*(\text{C1-C3})$  having energies 21.20 and 17.14, respectively.

Table-5 shows hybrid, polarization coefficient and atomic orbital contribution in selected natural bond orbitals of 4-HPP. It enlists natural hybrid orbitals  $h_A$  and  $h_B$ , the constituents of NBO, polarization coefficient  $c_A$  and  $c_B$ , atom and hybrid labels indicating percentage s and p character of atomic orbitals.

As evident from Table-5, the  $\sigma(\text{C1-C2})$  is formed from  $sp^{1.60}$  hybrid of carbon which has s(38.50%) p(61.46%) d(0.04%) character and  $sp^{1.95}$  hybrid carbon atom, which has s(33.83%) p(66.13%) d(0.04%) character. Thus, NBO 1 is a result of the overlapping of  $sp^{1.60}$  and  $sp^{1.95}$  of C1 and C2, respectively. The higher electronegativity of the C1 atom is reflected by its coefficient of polarization (0.7086) for the C2 hybrid. This can also be expressed as:

$$\sigma_{\text{CC}} = 0.7086(sp^{1.60})_{\text{C1}} + 0.7056(sp^{1.95})_{\text{C2}}$$

In Table-6, the direction of hybrids is stated by the polar ( $\theta$ ) and azimuthal ( $\phi$ ) angles of vectors, which describe its p

TABLE-4  
SECOND ORDER PERTURBATION THEORY OF THE FOCK MATRIX NBO ANALYSIS OF 4-HPP

Donor	Type	ED/e	Acceptor	Type	ED/e	E(2) (kcal/mol)	E(j)-E(i) (a.u.)	F(i,j) (a.u.)
C1-C2	$\sigma$	1.97934	C1-C3	$\sigma^*$	0.06834	2.00	1.16	0.044
			C1-N4	$\sigma^*$	0.02246	2.50	1.25	0.050
			C2-H5	$\sigma^*$	0.01257	3.36	1.47	0.063
			C2-C6	$\sigma^*$	0.01814	3.16	1.32	0.058
			C3-N7	$\sigma^*$	0.06148	1.57	1.25	0.040
C1-C3	$\sigma$	1.97332	C6-H10	$\sigma^*$	0.01181	1.81	1.46	0.046
			C1-C2	$\sigma^*$	0.03084	1.69	1.27	0.041
			C1-N4	$\sigma^*$	0.41800	1.17	1.19	0.033
			C2-C6	$\sigma^*$	0.27624	2.21	1.27	0.047
			C3-N7	$\sigma^*$	0.06148	0.79	1.20	0.028
			C3-O8	$\sigma^*$	0.01242	1.16	1.24	0.034
			N4-C9	$\sigma^*$	0.01804	3.51	1.18	0.058
C1-N4	$\sigma$	1.98637	N7-C12	$\sigma^*$	0.03522	4.66	1.06	0.063
			N7-H13	$\sigma^*$	0.01407	0.57	1.82	0.029
			C1-C2	$\sigma^*$	0.03084	2.73	1.43	0.056
			C1-C3	$\sigma^*$	0.06834	0.56	1.27	0.024
			C2-H5	$\sigma^*$	0.01257	1.14	1.58	0.038
			C3-O8	$\sigma^*$	0.34104	1.52	1.41	0.041
			N4-C9	$\sigma^*$	0.01804	0.83	1.35	0.030
C1-N4	$\pi$	1.71912	C9-H14	$\sigma^*$	0.01761	1.56	1.54	0.044
			C2-C6	$\pi^*$	0.27624	14.53	0.33	0.062
			C3-O8	$\pi^*$	0.34104	14.07	0.32	0.061
C2-H5	$\sigma$	1.97588	C9-C11	$\pi^*$	0.02543	22.43	0.33	0.077
			C1-C2	$\sigma^*$	0.03084	2.33	1.18	0.047
			C1-N4	$\sigma^*$	0.41800	5.42	1.11	0.069
C2-C6	$\sigma$	1.97678	C2-C6	$\sigma^*$	0.27624	1.83	1.18	0.042
			C6-H10	$\sigma^*$	0.01181	0.58	1.31	0.025
			C6-C11	$\sigma^*$	0.01934	3.16	1.17	0.054
			C1-C2	$\sigma^*$	0.03084	3.73	1.31	0.062
			C1-C3	$\sigma^*$	0.06834	3.14	1.15	0.054
			C2-H5	$\sigma^*$	0.06834	2.71	1.46	0.056
			C6-H10	$\sigma^*$	0.01181	2.36	1.44	0.052
C2-C6	$\pi$	1.62926	C6-C11	$\sigma^*$	0.01934	2.71	1.30	0.053
			C11-H15	$\sigma^*$	0.01239	2.16	1.44	0.050
			C1-N4	$\pi^*$	0.41800	29.67	0.27	0.080
			C9-C11	$\pi^*$	0.28345	19.00	0.29	0.068
			C3-C7	$\sigma$	1.98656	C1-C2	$\sigma^*$	0.03084
C3-C7	$\sigma$	1.98656	C1-C3	$\sigma^*$	0.06834	0.60	1.27	0.025
			C3-O8	$\sigma^*$	0.01242	1.12	1.41	0.035
			N7-C12	$\sigma^*$	0.03522	2.17	1.22	0.046
			N7-H13	$\sigma^*$	0.01407	5.61	1.99	0.094
			C12-C16	$\sigma^*$	0.02154	1.38	1.38	0.039
C3-O8	$\sigma$	1.99395	C1-C3	$\sigma^*$	0.06834	1.67	1.44	0.044
			C1-N4	$\sigma^*$	0.02246	1.43	1.53	0.042
			C3-N7	$\sigma^*$	0.06148	0.70	1.53	0.030
C3-O8	$\sigma$	1.97271	C1-N4	$\sigma^*$	0.41800	5.89	0.35	0.045
			C3-O8	$\sigma^*$	0.34104	0.99	0.36	0.018
N4-C9	$\sigma$	1.98579	C1-C3	$\sigma^*$	0.06834	2.95	1.25	0.055
			C1-N4	$\sigma^*$	0.41800	0.96	1.33	0.032
			C9-C11	$\sigma^*$	0.28345	1.91	1.43	0.047
			C9-H14	$\sigma^*$	0.01761	1.31	1.52	0.040
			C11-H15	$\sigma^*$	0.01239	1.25	1.54	0.039
C6-H10	$\sigma$	1.98159	C1-C2	$\sigma^*$	0.03084	3.23	0.20	0.056
			C2-H5	$\sigma^*$	0.01257	0.56	1.35	0.024
C6-H10	$\sigma$	1.98159	C2-C6	$\sigma^*$	0.27624	1.85	1.20	0.042
			C6-C11	$\sigma^*$	0.01934	1.62	1.19	0.039
			C9-C11	$\sigma^*$	0.02543	2.89	1.22	0.053
			C11-H15	$\sigma^*$	0.01239	0.54	1.33	0.024

C6-C11	$\sigma$	1.97917	C2-H5	$\sigma^*$	0.01257	2.17	2.46	0.050
			C2-C6	$\sigma^*$	0.01814	2.71	1.31	0.053
			C6-H10	$\sigma^*$	0.01181	2.32	1.44	0.052
			C9-C11	$\sigma^*$	0.02543	2.93	1.32	0.056
			C9-H14	$\sigma^*$	0.01761	1.72	1.42	0.044
N7-C12	$\sigma$	1.98419	C11-H15	$\sigma^*$	0.01239	2.70	1.44	0.056
			C1-C3	$\sigma^*$	0.06834	1.78	1.21	0.042
			C3-N7	$\sigma^*$	0.06148	2.64	1.30	0.053
			N7-H13	$\sigma^*$	0.01407	4.34	1.93	0.083
			C12-C17	$\sigma^*$	0.02000	1.12	1.41	0.035
N7-H13	$\sigma$		C16-C19	$\sigma^*$	0.01674	1.24	1.40	0.037
			C17-C20	$\sigma^*$	0.01794	1.65	1.36	0.042
			C3-N7	$\sigma^*$	0.06148	2.76	1.34	0.055
			C3-O8	$\sigma^*$	0.34104	5.87	1.39	0.081
			N7-C12	$\sigma^*$	0.03522	1.65	1.20	0.040
C9-C11	$\sigma$	1.97974	N7-H13	$\sigma^*$	0.01407	0.57	1.97	0.030
			C12-C17	$\sigma^*$	0.34716	1.95	1.45	0.047
			N4-C9	$\sigma^*$	0.01804	1.72	1.46	0.041
			C6-H10	$\sigma^*$	0.01181	2.07	1.44	0.049
			C6-C11	$\sigma^*$	0.01934	3.09	1.32	0.057
C9-C11	$\pi$	1.98355	C9-H14	$\sigma^*$	0.01761	2.72	1.44	0.056
			C11-H15	$\sigma^*$	0.01239	2.80	1.46	0.057
			C1-N4	$\pi^*$	0.41800	15.99	0.27	0.060
C9-H14	$\sigma$	1.98190	C2-C6	$\pi^*$	0.01814	19.93	0.30	0.071
			C1-N4	$\sigma^*$	0.41800	3.85	1.12	0.059
C11-H15	$\sigma$	1.97848	N4-C9	$\sigma^*$	0.01804	0.89	1.11	0.028
			C6-C11	$\sigma^*$	0.01934	3.77	1.18	0.060
			C9-C11	$\sigma^*$	0.02543	1.67	1.21	0.040
			C11-H15	$\sigma^*$	0.01239	0.64	1.33	0.026
			C2-C6	$\sigma^*$	0.01814	2.95	1.20	0.053
C12-C16	$\sigma$	1.97599	N4-C9	$\sigma^*$	0.01804	4.77	1.11	0.065
			C6-C11	$\sigma^*$	0.01934	1.65	1.18	0.039
			C9-C11	$\sigma^*$	0.02543	1.97	1.21	0.044
			C9-H14	$\sigma^*$	0.01761	0.69	1.31	1.027
			C3-N7	$\sigma^*$	0.06148	2.44	1.21	0.049
C12-C17	$\sigma$	1.97749	C12-C17	$\sigma^*$	0.34716	3.90	1.32	0.064
			C16-H18	$\sigma^*$	0.01112	2.73	1.14	0.056
			C16-C19	$\sigma^*$	0.01674	2.98	1.31	0.056
			C17-H21	$\sigma^*$	0.01222	2.12	1.46	0.050
			C19-H22	$\sigma^*$	0.01260	1.86	1.41	0.046
C12-C17	$\pi$	1.68180	N7-C12	$\sigma^*$	0.03522	0.80	1.11	0.027
			N7-H13	$\sigma^*$	0.01407	1.33	1.87	0.045
			C12-C16	$\sigma^*$	0.02154	3.75	1.27	0.061
			C16-H18	$\sigma^*$	0.01112	1.61	1.45	0.043
			C17-C20	$\sigma^*$	0.01794	3.03	1.30	0.056
C16-H18	$\sigma$	1.97894	C17-H21	$\sigma^*$	0.01222	3.76	1.49	0.067
			C20-H24	$\sigma^*$	0.01154	1.36	1.46	0.040
			C16-C19	$\pi^*$	0.01674	19.27	0.29	0.067
C16-C19	$\sigma$	1.96775	C20-H24	$\pi^*$	0.01154	17.42	0.30	0.065
			N7-C12	$\sigma^*$	0.03522	0.61	0.97	0.022
			C12-C16	$\sigma^*$	0.02154	1.35	1.13	0.035
			C12-C17	$\sigma^*$	0.34716	3.27	1.22	0.056
			C16-C19	$\sigma^*$	0.01674	2.21	1.21	0.046
C16-C19	$\pi$	1.74090	C19-H22	$\sigma^*$	0.01260	0.58	1.31	0.025
			C19-C23	$\sigma^*$	0.03003	3.36	1.18	0.056
			N7-C12	$\sigma^*$	0.03522	3.89	1.09	0.058
			C12-C16	$\sigma^*$	0.02154	3.31	1.25	0.058
			C16-H18	$\sigma^*$	0.01112	2.91	1.44	0.058
C16-C19	$\pi$	1.74090	C19-H22	$\sigma^*$	0.01260	3.22	1.43	0.061
			C19-C23	$\sigma^*$	0.03003	3.73	1.30	0.062
			C23-O25	$\sigma^*$	0.02894	4.58	1.03	0.061
C16-C19	$\pi$	1.74090	C12-C17	$\pi^*$	0.34716	15.57	0.31	0.064
			C20-C23	$\pi^*$	0.33822	19.40	0.31	0.070

C17–C20	$\sigma$	1.96593	N7–C12	$\sigma^*$	0.03522	5.03	1.05	0.065
			C12–C17	$\sigma^*$	0.34716	3.64	1.30	0.062
			C17–H21	$\sigma^*$	0.01222	2.36	1.44	0.052
			C20–C23	$\sigma^*$	0.01154	3.35	1.31	0.059
			C20–H24	$\sigma^*$	0.01154	2.43	1.41	0.053
C17–H21	$\sigma$	1.97613	C23–O25	$\sigma^*$	0.02894	4.88	0.99	0.062
			N7–C12	$\sigma^*$	0.03522	0.78	0.95	0.024
			C12–C16	$\sigma^*$	0.02154	4.38	1.11	0.062
			C12–C17	$\sigma^*$	0.34716	2.52	1.20	0.049
			C17–C20	$\sigma^*$	0.01794	1.67	1.15	0.039
C19–H22	$\sigma$	1.97683	C20–C23	$\sigma^*$	0.01154	2.73	1.20	0.051
			C20–H24	$\sigma^*$	0.01154	0.53	1.30	0.023
			C12–C16	$\sigma^*$	0.02154	3.79	1.13	0.059
			C16–H18	$\sigma^*$	0.01112	0.60	1.32	0.025
			C16–C19	$\sigma^*$	0.01674	2.44	1.21	0.049
C19–C23	$\sigma$	1.97945	C19–C23	$\sigma^*$	0.03003	1.84	1.18	0.042
			C20–C23	$\sigma^*$	0.01154	3.51	1.23	0.059
			C23–O25	$\sigma^*$	0.02894	0.67	0.91	0.022
			C16–H18	$\sigma^*$	0.01112	1.78	1.44	0.045
			C16–C19	$\sigma^*$	0.01674	3.61	1.33	0.062
C20–C23	$\sigma$	1.97968	C19–H22	$\sigma^*$	0.01260	3.15	1.43	0.060
			C20–C23	$\sigma^*$	0.33822	4.26	1.35	0.068
			C20–H24	$\sigma^*$	0.01154	1.91	1.45	0.047
			C17–C20	$\sigma^*$	0.01794	3.00	1.30	0.056
			C17–C21	$\sigma^*$	0.01222	1.38	1.49	0.041
C20–C23	$\pi$	1.68382	C19–H22	$\sigma^*$	0.01260	1.81	1.44	0.046
			C19–C23	$\sigma^*$	0.03003	4.10	1.31	0.066
			C20–H24	$\sigma^*$	0.01154	3.68	1.46	0.066
			C12–C17	$\pi^*$	0.34716	19.16	0.31	0.069
			C16–C19	$\pi^*$	0.01674	20.03	0.30	0.069
C20–H24	$\sigma$	1.97700	O25–H26	$\pi^*$	0.00267	0.56	1.12	0.024
			C12–C17	$\sigma^*$	0.34716	3.13	1.21	0.055
			C17–C20	$\sigma^*$	0.01794	1.67	1.16	0.039
			C19–C23	$\sigma^*$	0.03003	4.19	1.17	0.062
			C20–C23	$\sigma^*$	0.01154	2.58	1.22	0.050
C23–O25	$\sigma$	1.99260	C23–O25	$\sigma^*$	0.02894	0.94	0.89	0.026
			C16–C19	$\sigma^*$	0.01674	1.23	1.46	0.038
			C17–C20	$\sigma^*$	0.01794	1.79	1.42	0.045
			C20–C23	$\sigma^*$	0.01154	0.52	1.48	0.025
			O25–H26	$\sigma^*$	0.00267	0.88	1.70	0.035
O25–H26	$\sigma$	1.98721	C20–C23	$\sigma^*$	0.01154	2.34	1.52	0.053
			C20–C23	$\sigma^*$	0.33822	1.49	0.92	0.036
N4	LP(1)	1.92867	C1–C2	$\sigma^*$	0.03084	8.97	0.96	0.084
			C1–C3	$\sigma^*$	0.06834	3.14	0.80	0.045
			N7–H13	$\sigma^*$	0.01407	1.37	1.52	0.041
			C9–C11	$\sigma^*$	0.02543	7.42	0.98	0.077
			C9–H14	$\sigma^*$	0.01761	3.58	1.07	0.056
N7	LP(1)	1.63864	C3–O8	$\pi^*$	0.34104	74.82	0.28	0.129
			C12–C17	$\pi^*$	0.34716	28.59	0.31	0.084
O8	LP(1)	1.98255	C1–C3	$\sigma^*$	0.06834	1.61	1.12	0.038
			C3–N7	$\sigma^*$	0.06148	0.96	1.21	0.031
O8	LP(2)	1.89243	C1–C3	$\pi^*$	0.06834	17.14	0.68	0.097
			C1–N4	$\sigma^*$	0.41800	0.64	0.76	0.020
			C3–N7	$\pi^*$	0.06148	21.10	0.77	0.115
			C17–H21	$\sigma^*$	0.01222	0.60	1.01	0.023
			C19–C23	$\sigma^*$	0.02545	5.43	1.16	0.071
O25	LP(1)	1.97778	C20–C23	$\sigma^*$	0.33822	0.53	1.21	0.023
			C19–C23	$\sigma^*$	0.03003	1.01	0.94	0.028
O25	LP(2)	1.92055	C20–C23	$\sigma^*$	0.02545	2.39	0.99	0.044
			C20–C23	$\pi^*$	0.33822	13.69	0.39	0.070

TABLE-5  
HYBRID, POLARIZATION COEFFICIENT AND ATOMIC ORBITAL  
CONTRIBUTION IN SELECTED NATURAL BOND ORBITALS OF 4-HPP

Bond orbital	Hybrid A ( $h_A$ )	Atomic orbital (%)	Polarization coefficient ( $C_A$ )	Hybrid B ( $h_B$ )	Atomic orbital (%)	Polarization coefficient ( $C_B$ )
$\sigma$ C1–C2	$sp^{1.60}$	s(38.50%) p(61.46%) d(0.04%)	0.7086	$sp^{1.95}$	s(33.83%) p(66.13%) d(0.04%)	0.7056
$\sigma$ C1–C3	$sp^{2.18}$	s(31.45%) p(68.50%) d(0.05%)	0.7155	$sp^{1.77}$	s(36.06%) p(63.90%) d(0.04%)	0.6986
$\sigma$ C1–N4	$sp^{2.33}$	s(30.04%) p(69.86%) d(0.09%)	0.6442	$sp^{1.78}$	s(35.91%) p(69.86%) d(0.09%)	0.7649
$\pi$ C1–N4	$sp^{1.00}$	s(0.00%) p(99.90%) d(0.10%)	0.6485	$sp^{1.00}$	s(0.0%) p(99.87%) d(0.12%)	0.7612
$\sigma$ C2–H5	$sp^{2.11}$	s(32.15%) p(67.80%) d(0.05%)	0.7732	$sp^{0.00}$	s(99.96%) p(0.04%)	0.6341
$\sigma$ C2–C6	$sp^{1.95}$	s(33.92%) p(66.04%) d(0.03%)	0.7088	$sp^{1.97}$	s(33.64%) p(66.33%) d(0.04%)	0.7054
$\pi$ C2–C6	$sp^{1.00}$	s(0.00%) p(99.96%) d(0.04%)	0.7013	$sp^{1.00}$	s(0.00%) p(99.96%) d(0.04%)	0.7039
$\sigma$ C3–N7	$sp^{2.07}$	s(32.53%) p(67.38%) d(0.10%)	0.6126	$sp^{2.14}$	s(31.83%) p(68.12%) d(0.05%)	0.7904
$\sigma$ C3–O8	$sp^{2.19}$	s(31.26%) p(68.60%) d(0.14%)	0.6043	$sp^{1.63}$	s(38.10%) p(61.88%) d(0.12%)	0.7967
$\pi$ C3–O8	$sp^{1.00}$	s(0.00%) p(99.61%) d(0.39%)	0.5429	$sp^{1.00}$	s(0.00%) p(99.90%) d(0.10%)	0.8398
$\sigma$ N4–C9	$sp^{1.88}$	s(34.64%) p(65.28%) d(0.08%)	0.7696	$sp^{2.32}$	s(30.08%) p(69.84%) d(0.08%)	0.6386
$\sigma$ C6–H10	$sp^{2.04}$	s(32.90%) p(67.04%) d(0.06%)	0.7655	$sp^{0.00}$	s(99.95%) p(0.05%)	0.6434
$\sigma$ C6–C11	$sp^{2.00}$	s(33.53%) p(66.61%) d(0.03%)	0.7061	$sp^{1.97}$	s(33.69%) p(66.28%) d(0.03%)	0.7081
$\sigma$ N7–C12	$sp^{1.85}$	s(35.05%) p(64.93%) d(0.02%)	0.7879	$sp^{2.78}$	s(26.40%) p(73.50%) d(0.09%)	0.6158
$\sigma$ N7–H13	$sp^{2.05}$	s(32.79%) p(67.14%) d(0.06%)	0.8143	$sp^{0.00}$	s(99.89%) p(0.02%)	0.5850
$\sigma$ C9–C11	$sp^{1.71}$	s(36.83%) p(63.14%) d(0.04%)	0.7017	$sp^{1.92}$	s(34.19%) p(65.77%) d(0.04%)	0.7125
$\pi$ C9–C11	$sp^{1.00}$	s(0.00%) p(99.96%) d(0.04%)	0.6911	$sp^{1.00}$	s(0.00%) p(99.69%) d(0.03%)	0.7228
$\sigma$ C9–H14	$sp^{2.03}$	s(33.02%) p(66.92%) d(0.06%)	0.7614	$sp^{0.00}$	s(99.95%) p(0.05%)	0.6843
$\sigma$ C11–H15	$sp^{2.12}$	s(32.03%) p(67.92%) d(0.05%)	0.7663	$sp^{0.00}$	s(99.96%) p(0.04%)	0.6425
$\sigma$ C12–C16	$sp^{1.82}$	s(35.51%) p(64.46%) d(0.04%)	0.7118	$sp^{2.04}$	s(32.92%) p(67.04%) d(0.04%)	0.7024
$\sigma$ C12–C17	$sp^{1.63}$	s(37.97%) p(62.00%) d(0.04%)	0.7115	$sp^{1.63}$	s(34.28%) p(65.68%) d(0.04%)	0.7027
$\pi$ C12–C17	$sp^{1.00}$	s(0.00%) p(99.97%) d(0.03%)	0.7221	$sp^{1.00}$	s(0.00%) p(99.95%) d(0.05%)	0.6918
$\sigma$ C16–H18	$sp^{2.15}$	s(31.72%) p(68.22%) d(0.025%)	0.7655	$sp^{0.00}$	s(99.69%) p(0.04%)	0.6434
$\sigma$ C16–C19	$sp^{1.84}$	s(35.22%) p(64.74%) d(0.03%)	0.7058	$sp^{1.87}$	s(34.79%) p(65.18%) d(0.03%)	0.7084
$\pi$ C16–C19	$sp^{99.99}$	s(0.01%) p(96.99%) d(0.03%)	0.7018	$sp^{99.99}$	s(0.01%) p(99.95%) d(0.03%)	0.7124
$\sigma$ C17–C20	$sp^{2.01}$	s(33.23%) p(66.74%) d(0.03%)	0.7069	$sp^{2.02}$	s(33.15%) p(66.82%) d(0.03%)	0.7073
$\sigma$ C17–H21	$sp^{2.08}$	s(32.04%) p(67.54%) d(0.05%)	0.7757	$sp^{0.00}$	s(99.95%) p(0.05%)	0.6311
$\sigma$ C19–H22	$sp^{2.15}$	s(31.76%) p(68.19%) d(0.05%)	0.7670	$sp^{0.00}$	s(99.96%) p(0.04%)	0.6416
$\sigma$ C19–C23	$sp^{2.00}$	s(33.33%) p(66.63%) d(0.04%)	0.7109	$sp^{1.67}$	s(37.47%) p(62.49%) d(0.04%)	0.7033
$\sigma$ C20–C23	$sp^{1.91}$	s(34.14%) p(65.55%) d(0.04%)	0.7088	$sp^{1.61}$	s(38.23%) p(61.73%) d(0.04%)	0.7054
$\pi$ C20–C23	$sp^{1.00}$	s(0.00%) p(99.95%) d(0.05%)	0.7094	$sp^{1.00}$	s(0.01%) p(99.95%) d(0.04%)	0.7048
$\sigma$ C20–H24	$sp^{2.09}$	s(32.32%) p(67.63%) d(0.05%)	0.7690	$sp^{0.00}$	s(99.96%) p(0.04%)	0.6393
$\sigma$ C23–O25	$sp^{3.14}$	s(24.08%) p(75.69%) d(0.23%)	0.5795	$sp^{2.56}$	s(28.07%) p(71.84%) d(0.09%)	0.8150
$\sigma$ C25–H26 (34)	$sp^{2.58}$	s(27.90%) p(71.97%) d(0.09%)	0.8453	$sp^{0.00}$	s(99.96%) p(0.04%)	0.5343
LP(1) N4	$sp^{2.39}$	s(23.50%) p(70.44%) d(0.06%)	–	–	–	–
LP(1) N7	$sp^{99.99}$	s(0.19%) p(99.73%) d(0.02%)	–	–	–	–
LP(1) O8	$sp^{0.61}$	s(62.02%) p(37.97%) d(0.01%)	–	–	–	–
LP(2) O8	$sp^{99.99}$	s(0.02%) p(99.91%) d(0.06%)	–	–	–	–
LP(1) O25	$sp^{1.57}$	s(38.88%) p(61.07%) d(0.05%)	–	–	–	–
LP(2) O25	$sp^{18.30}$	s(5.18%) p(94.57%) d(0.07%)	–	–	–	–

component. The direction of hybrid is correlated to maximum amplitude and compared to corresponding line of centers between the nuclei. The bend in bond is achieved when expressed as deviation angles between the two atoms. The  $\sigma_{CC}$  bond (NBO1) is away from the line of the C–C center by  $1.2^\circ$ . Similarly,  $\sigma_{CN}$  is bent away from the line of center of C–N by  $1.6^\circ$ .

**Population analysis:** Analysis of atomic charges is an essential analysis because it is accountable for dipole moment, molecular reactivity and electronic structure also provides cardinal statistics for the NMR chemical shifts of the atom. Charges on the atoms were calculated by Mulliken population analysis (MPA) using the B3LYP/6-311 ++G(d,p) method and basis set. The corresponding graph is shown in Fig. 5.

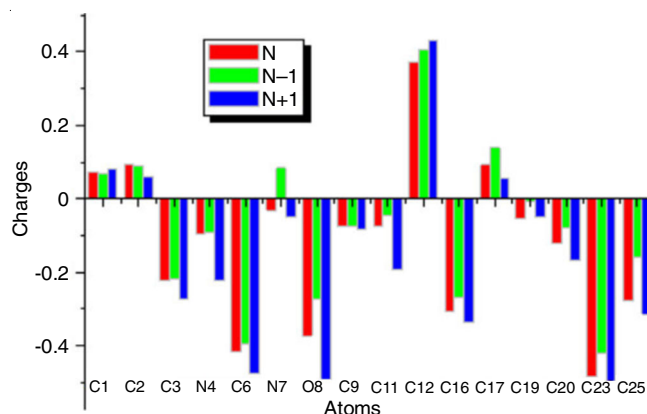


Fig. 5. Mulliken atomic charges of atoms of 4-HPP

TABLE-6  
NATURAL HYBRID ORBITAL DIRECTIONALITY  
AND BOND BENDING (DEVIATIONS FROM  
LINE OF NUCLEAR CENTRES) OF 4-HPP

Bond orbital	Deviation angle (°)		Line of centers	
	Hybrid A	Hybrid B	Polar (θ)	Azimuthal (φ)
σ C1–C2	1.1	1.2	91.1	139.4
σ C1–N4	2.5	1.6	87.8	261.3
π C1–N4	90.2	90.2	87.8	261.3
σ C2–C6	2.0	1.1	88.3	199.0
π C2–C6	90.2	90.1	88.3	199.0
σ C3–N7	4.9	9.3	86.4	314.6
σ C3–O8	90.4	89.8	93.1	77.8
σ N4–C9	1.2	3.7	88.4	198.6
σ C6–C11	–	1.2	87.9	261.4
σ N7–C12	2.8	–	90.3	3.2
σ N7–H13	6.7	–	92.5	238.2
σ C9–C11	4.3	2.2	91.1	141.3
π C9–C11	90.0	90.1	91.1	141.3
σ C9–H14	1.2	–	87.3	259.9
σ C12–C16	2.5	–	94.5	303.2
σ C12–C17	2.4	1.2	86.6	61.2
σ C12–C17	90.0	86.9	86.5	61.2
σ C16–C19	2.8	2.1	90.8	2.5
σ C16–C19	89.8	89.2	90.8	2.5
σ C17–C20	2.5	2.0	89.3	2.0
σ C17–H21	1.4	–	87.2	121.7
σ C19–C23	–	6.1	85.2	62.3
σ C20–C23	1.4	5.3	95.2	302.2
σ C20–C23	90.2	89.5	95.2	302.2
σ C23–O25	–	5.6	91.4	3.3
σ O25–H26	5.6	–	52.1	288.4
π* C1–N4	90.2	90.2	87.8	261.3
π* C2–C6	90.0	90.1	88.3	199.0
σ* C3–O8	90.4	89.8	93.1	77.8
π* C9–C11	90.0	90.1	91.1	141.3
σ* C12–C17	90.8	86.6	86.6	61.2
σ* C16–C19	89.8	89.2	90.8	2.5
σ* C20–C23	90.2	89.5	95.2	302.2

*N*-(4-hydroxyphenyl)picolinamide (4-HPP) molecule has 26 atoms and twelve carbon, two nitrogen and two oxygen. Apart from C1, C2 and C17, all the carbon atoms are negatively charged; nitrogen and oxygen also have a negative charge. C23 is the most negatively charged atom connected to the hydroxyl group. Out of the three positive atoms, C2 is the most positively charged atom. C1 is connected with two carbon and a nitrogen atom. C17 is connected with two carbon and a hydrogen atom. The hydrogen atoms have an equal positive charge but with a slight deviation depending on their attachment with carbon, nitrogen or oxygen.

The Fukui function can be easily evaluated from tools like Mulliken population analysis or NBO analysis that comes along with most quantum chemistry calculations. With the increase in the value of the Fukui function, the reactivity of the site also increases with a decrease in electron density. The  $fr^+$  function measures the change in electron density followed by the addition of an electron. Larger the  $fr^+$  value at site  $r$  indicates that it can accept more electrons during the nucleophilic (electron gain) attack. Hence, the molecule is vulnerable to a nucleophilic attack where there is a high value of  $fr^+$ . Likewise, the molecule is more likely to have an electrophilic attack where it has a greater value of  $fr^-$  and the electron density increases.

From Table-7, it is evident that the order for electrophilic attack is  $N4 > C11 > O8 > C6 > C3 > C20$  while for nucleophilic attack, it is  $O25 > N7 > O8 > C11 > C16 > C12 > C6$ . The position of reactive nucleophilic and electrophilic sites is in agreement with the chemical behaviour and total electron density surface. The information regarding chemical softness can also be derived from the Fukui functions, which is an important factor for determining biological activity like ligand-protein interactions of the molecule [58,59].

**Frontier molecular orbital (FMO) theory analysis:** The highest occupied molecular orbital (HOMO) and lowest unoccupied molecular orbital (LUMO) are used to assess molecule stability and reactivity (LUMO). The HOMO ( $E_{HOMO}$ ) energy

TABLE-7  
MULLIKEN CHARGE DISTRIBUTION, FUKUI FUNCTION AND LOCAL SOFTNESS  
CORRESPONDING TO (0,1), (-1,2) AND (1,2) CHARGE AND MULTIPLICITY OF 4-HPP

Atom	Mulliken atomic charges			Fukui functions				Local softness		
	N (0,1)	N-1 (+1,2)	N+1 (-1,2)	$Fr_+$	$fr_-$	$\Delta f$	$fr_0$	$sr_+ fr_+$	$sr_- fr_-$	$sr_0 fr_0$
C1	0.072503	0.066526	0.082071	0.009568	0.005977	0.003591	0.048808	0.004936	0.003084	0.02518
C2	0.095578	0.088582	0.058476	-0.037102	0.006996	-0.044098	0.014185	-0.01914	0.003609	0.007318
C3	-0.222674	-0.218485	-0.274196	-0.051522	-0.004189	-0.047333	-0.1649535	-0.02658	-0.00216	-0.0851
N4	-0.095684	-0.093256	-0.223425	-0.127741	-0.002428	-0.125313	-0.176797	-0.0659	-0.00125	-0.09121
C6	-0.415392	-0.394531	-0.477074	-0.061682	-0.020861	-0.040821	-0.2798085	-0.03182	-0.01076	-0.14435
N7	-0.031462	0.083510	-0.048768	-0.017306	-0.114972	0.097666	-0.090523	-0.00893	-0.05931	-0.0467
O8	-0.373195	-0.274187	-0.490846	-0.117651	-0.099008	-0.018643	-0.3537525	-0.0607	-0.05108	-0.1825
C9	-0.075179	-0.073283	-0.082295	-0.007116	-0.001896	-0.00522	-0.0456535	-0.00367	-0.00098	-0.02355
C11	-0.073400	-0.045726	-0.194700	-0.1213	-0.027674	-0.093626	-0.171837	-0.06258	-0.01428	-0.08865
C12	0.373685	0.407145	0.431433	0.057748	-0.03346	0.091208	0.2278605	0.029792	-0.01726	0.117552
C16	-0.305098	-0.268981	-0.336595	-0.031497	-0.036117	0.00462	-0.2021045	-0.01625	-0.01863	-0.10426
C17	0.091983	0.138707	0.054326	-0.037657	-0.046724	0.009067	-0.0150275	-0.01943	-0.0241	-0.00775
C19	-0.054710	-0.008270	-0.049607	0.005103	-0.04644	0.051543	-0.045472	0.002633	-0.02396	-0.02346
C20	-0.121754	-0.077304	-0.167626	-0.045872	-0.04445	-0.001422	-0.128974	-0.02367	-0.02293	-0.06654
C23	-0.483985	-0.420475	-0.497413	-0.013428	-0.06351	0.050082	-0.2871755	-0.00693	-0.03276	-0.14815
O25	-0.277489	-0.158988	-0.313163	-0.035674	-0.118501	0.082827	-0.233669	-0.0184	-0.06113	-0.12055

is proportional to the ionization potential (IP), while the LUMO ( $E_{\text{LUMO}}$ ) energy is utilized to calculate electron affinity (EA). If  $E_{\text{HOMO}} \approx \text{IP}$  and  $E_{\text{LUMO}} \approx \text{EA}$ , then electronegativity is related to the average value of HOMO and LUMO [60]. Atomic orbital HOMO-LUMO of frontier molecular orbital of 4-HPP is shown in Fig. 6.

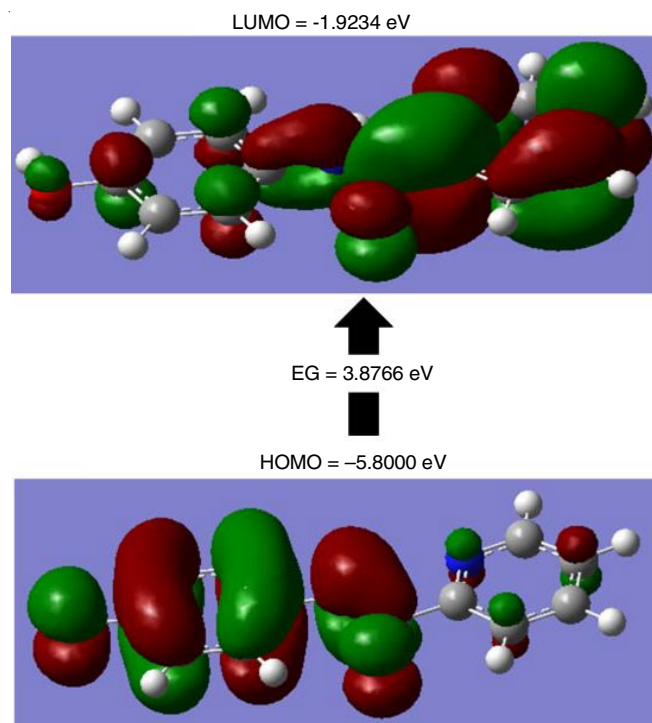


Fig. 6. Atomic orbital HOMO-LUMO of frontier molecular orbital of 4-HPP

HOMO and LUMO have a 3.8768 energy difference. The molecule's chemical hardness is 1.9384, indicating that it is stable and its global softness is 0.51589, indicating that it is non-toxic. The electrophilicity index is 3.8466, whereas the electronegativity is 3.616 due to the presence of nitrogen and oxygen atoms. During electron transfer, the electrophile's ability to gain electrons usually results in a drop in total energy. The calculated values are given in Table-8. As explained in Conceptual DFT (CDFT) [61], parameters including electrophilicity, hardness and chemical potential are used to quantify biology and identify reactive sites. The electrophilicity index is the most important metric for studying biological activities [62] and it's also utilized to predict toxicological behaviour [63]. The

TABLE-8  
CALCULATED ENERGY VALUES OF  
4-HPP BY B3LYP/6-311++G(d,p)

Parameter	Values
$E_{\text{HOMO}}$ (eV)	-5.8000
$E_{\text{LUMO}}$ (eV)	-1.9234
Ionization potential	5.8000
Electron affinity	1.9234
Energy gap (eV)	3.8766
Electronegativity	3.8616
Chemical potential	-3.8616
Chemical hardness	1.9384
Chemical softness	0.51589
Electrophilicity index	3.8466

toxic potential of a chemical can be determined using electrophilic reactivity [64].

**NMR spectral analysis:**  $^1\text{H}$  &  $^{13}\text{C}$  chemical shift calculations were done by gauge independent atomic orbital theory (GIAO) employing B3LYP/6311++G(d,p) basis set. The shifts are calculated for the DMSO solvent phase and the values are given in Table-9.

TABLE-9  
EXPERIMENTAL AND THEORETICAL  
 $^{13}\text{C}$  AND  $^1\text{H}$  CHEMICAL SHIFT VALUES OF 4-HPP

Atoms	Experimental chemical shift (ppm)	Calculated chemical shift (ppm) B3LYP/6311++G(d,p)	Group
C20	115	118.406	C-H
C19	115	119.509	C-H
C17	122	123.449	C-H
C16	122	123.888	C-H
C2	124	126.957	C-H
C11	127	132.132	C-H
C12	130	138.095	C-N
C6	140	143.621	C-H
C1	147	156.03	C-C
C9	152	154.097	C-H
C23	155	160.547	C-O
C3	163	165.879	C=O
H26	5.6	5.52863	O-H
H22	6.7	7.131	C-H
H24	6.7	7.2249	C-H
H18	6.8	7.3875	C-H
H10	7.8	8.31091	C-H
H21	7.8	9.09335	C-H
H15	8.2	7.924	C-H
H5	8.4	8.73107	C-H
H14	8.6	7.9243	C-H
H13	10.5	9.09335	N-H

The overall observation for  $^{13}\text{C}$  NMR shows the shifts of all the carbons are above 100 ppm. C12 which is attached to a nitrogen atom has 138.09 ppm and the experimental value is 130. C3 of carbonyl group shows shift at 163 experimentally and at 165.879 theoretically, it has the highest shift among all the carbons present in the molecule, afar from TMS reference while the peak at 155 and 154.09 experimentally and theoretically, respectively assigned to C23 attached to C-O group gave the second-highest shift

The  $^1\text{H}$  NMR spectra was recorded between 5.6 and 10.5 ppm experimentally and between 5 and 9.09 theoretically. H13 attached to the nitrogen atoms shows the highest chemical shift at 10.5 experimentally and 9.09 theoretically and H26 of hydroxyl group has the lowest shift at 5.56 experimentally and 5.52 theoretically which is closest to TMS. The graph of NMR shift is shown in Figs. 7 and 8.

**Thermodynamical properties:** Fundamental thermodynamical parameters like free energy (G), entropy (S) and enthalpy (H) for 4-HPP were calculated based on vibrational analysis at various temperatures ranging from 100 K to 500 K using B3LYP/6311++G(d,p) method and basis set. The values for these functions are tabulated in Table-10.

As evident from Fig. 9, thermodynamic functions increase with the increase in temperature because molecular vibrational intensities increase with the rise in temperature accompanied

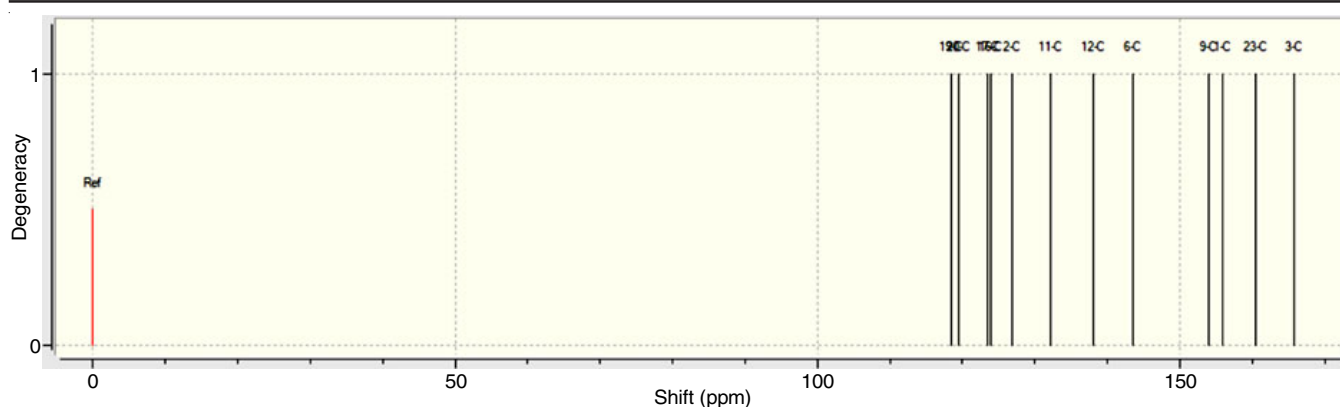
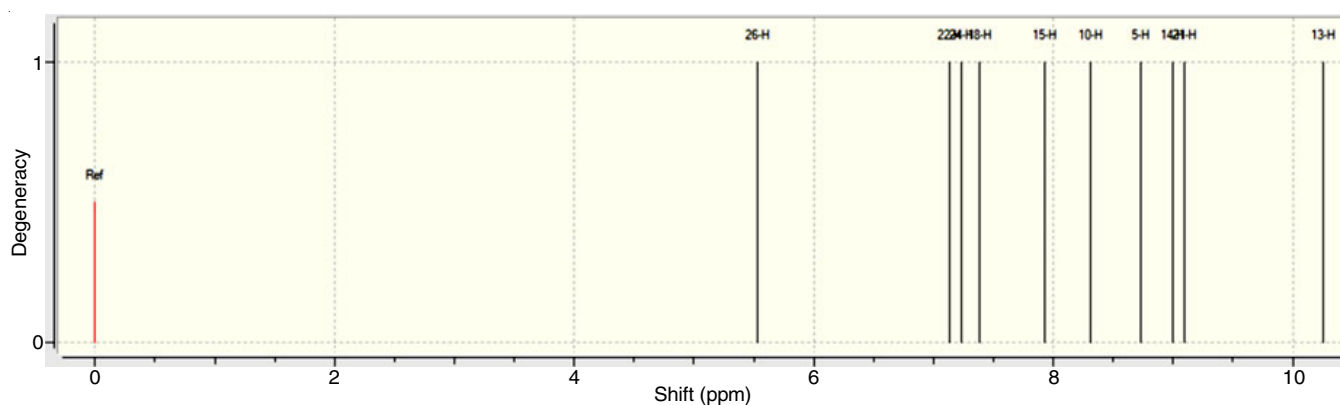
Fig. 7. Calculated  $^{13}\text{C}$  NMR of 4-HPPFig. 8. Calculated  $^1\text{H}$  NMR of 4-HPP

TABLE-10  
TEMPERATURE DEPENDENCE OF THERMODYNAMIC  
PROPERTIES OF 4-HPP AT B3LYP/6-311++G(d,p)

T (K)	$G_{p,m}^0 \times 10$ (J/mol K)	$S_m^0$ (J/mol K)	$H_m^0$ (kJ/mol)
100	508.203	312.791	539.482
200	237.309	382.804	551.179
300	144.778	450.196	569.393
400	96.8348	517.508	594.342
500	66.7385	583.208	625.297

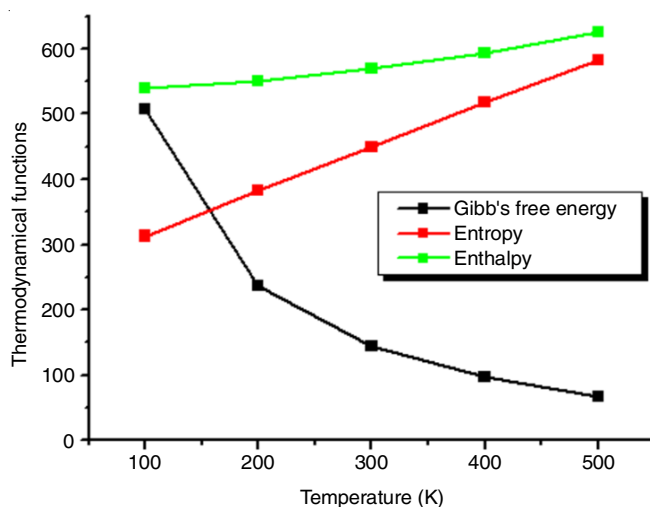


Fig. 9. Graph representing dependence of Gibbs free energy, entropy and enthalpy on temperature of 4-HPP

by an increase in translational and rotational energy according to the equipartition theorem [60,61]. Free energy decreases

while the enthalpy and entropy of the system increase with the temperature rise.

Quadratic and linear formulae are used to fit the correlation equations between these thermodynamic functions and temperatures. This thermodynamic data can be used to determine other thermodynamic energies and the direction of chemical reactions according to the second law of thermodynamics [65]. The corresponding fitting factors ( $R^2$ ) and fitting equations for these parameters are as follows:

$$G_{p,m}^0 = 0.0038T^2 - 3.2785T + 780.8852 \quad R^2 = 0.823$$

$$S_m^0 = -0.0001T^2 + 0.7128T + 242.287 \quad R^2 = 1.000$$

$$H_m^0 = 0.0003T^2 + 0.0209T + 534.1262 \quad R^2 = 0.969$$

**Intermolecular interactions:** To examine interactions between atoms in a crystal of 4-HPP, Hirshfeld analysis and 2-D fingerprint plot were drawn [66]. Hirshfeld surfaces can be analyzed in crystals only. Hirshfeld surface of 4-HPP mapped with  $d_{\text{norm}}$ ,  $d_i$ ,  $d_e$ , shape index and curvedness are shown in Fig. 10a-e, respectively. It was found that the  $d_{\text{norm}}$  value comes from  $-0.5465$  to  $1.3142 \text{ \AA}$ , shape index varies from  $-0.9787$  to  $0.9979 \text{ \AA}$ , curvedness from  $-3.5865$  to  $0.1650 \text{ \AA}$  was attained as minimal to maximal value, respectively. Interaction of 4-HPP with neighboring molecules and the bond length of H-bond neighboring atoms are  $3.118 \text{ \AA}$ ,  $4.445 \text{ \AA}$ ,  $4.421 \text{ \AA}$  as shown in Fig. 10. And corresponding surface property information is listed in Table-11. From this table, the surface is mapped over a  $d_{\text{norm}}$  ( $-0.5465$  to  $1.3142$ ),  $d_i$  ( $0.7808$  to  $2.4124$ ),  $d_e$  ( $0.7808$  to  $2.4210$ ), shape index ( $-0.9787$  to  $0.9979$ ), curvedness ( $-3.5865$  to  $0.1650$ ), fragment path (0 to 13). The above-

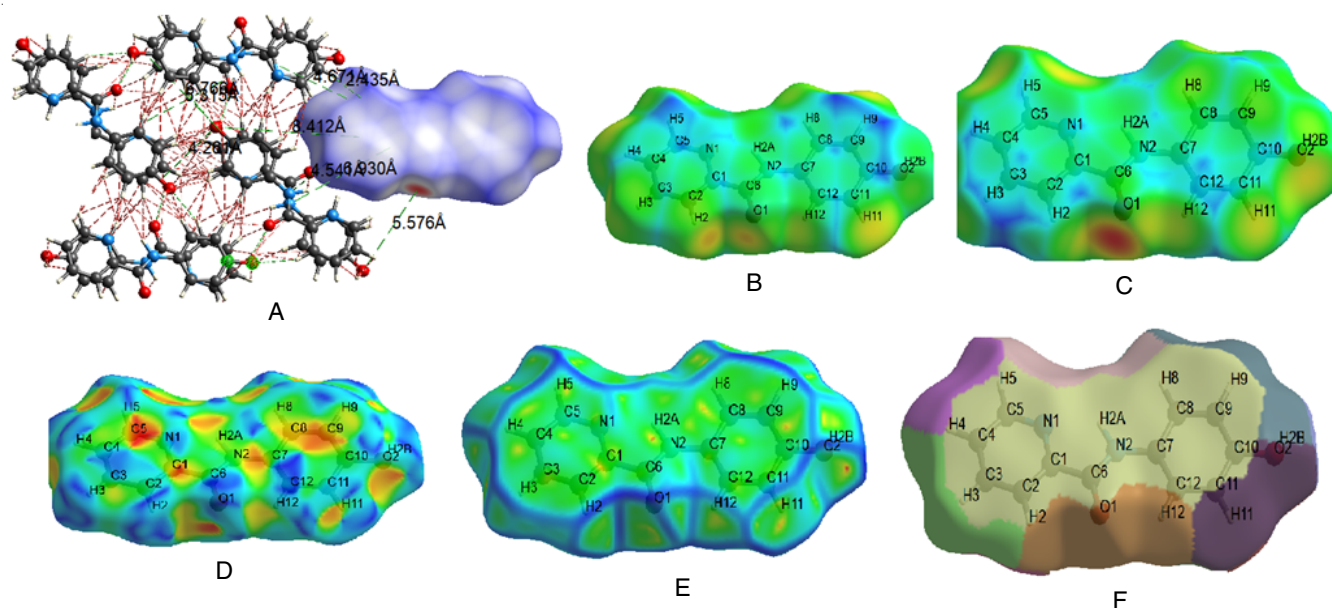


Fig. 10. Hirshfeld surface for 4-HPP mapped with  $d_{\text{norm}}$  (A),  $d_i$  (B),  $d_e$  (C), shape index (D) and curvedness (E), Fragment patch (F)

TABLE-11  
SURFACE PROPERTY INFORMATION  
IN HIRSHFELD FOR 4-HPP

Mode	Minimum interaction	Mean interaction	Maximum interaction
$d_{\text{norm}}$	-0.5465	0.4821	1.3142
$d_i$	0.7808	1.6909	2.4124
$d_e$	0.7808	1.7073	2.4210
Shape index	-0.9787	0.2823	0.9979
Curvedness	-3.5865	-1.0400	0.1650
Fragment patches	0	6.6793	13

mentioned description can be described by the colour code as follows: Red spots indicate the close contact with the neighbouring molecules, blue indicates longer contact, white represents the contact around van der Waals separation [67-69]. In this crystal, both inside and outside intermolecular interactions have contributed to overall molecule in full 2-D fingerprint interaction and it has been visualized at the  $d_{\text{norm}}$  on the Hirshfeld surface with a neighboring molecule which can be connected by H-H (45.6%), H-O (18.6%), C-H (15%), for the title molecule and have been shown in Fig. 11 and the values are listed in Table-12. These 2-D fingerprint interaction  $d_e$  and  $d_i$  graphical values are in good agreement for intermolecular interactions in the donor and acceptor regions of the fingerprint obtained from Hirshfeld analysis are in good connection with the single crystal analysis.

**Molecular docking:** Molecular docking in 3D can quickly estimate the protein-ligand interaction location. This method allows us to see the specific location of the bond and how it interacts. The optimal binding energy is calculated by docking the specified molecule (ligand) with the appropriate protein.

TABLE-12  
FINGERPRINT PERCENTAGE OF THE TOTAL SURFACE  
AREA FOR CLOSED CONTACT BETWEEN ATOMS  
INSIDE AND OUTSIDE THE SURFACE FOR 4-HPP

Atom	Inside atom outside atom (%)			
	C	H	N	O
C	10.1	8.6	2.1	0.3
H	6.5	45.6	1.8	8.6
N	2.1	2.5	0.4	0.3
O	0.3	10.5	0.3	-

The SwissADME program, which predicts drug targets online, is used to choose the best protein. The ligand is docked with 5ZWJ, a transferase enzyme, in this study utilizing Chimera 1.14 [40] and Autodock Vina software [38,39]. The drug has strong contact with the protein, as demonstrated by the binding energy of -5.7 kcal/mol and the hydrogen bond distance of 2.273 Å, showing that this ligand is suitable for the protein under consideration. The protein 5G0N has 3 residues in its structure with a  $K_i$  value of 6603. Ligand 4-HPP embedded in the active site of 5ZWJ protein shown in Fig. 12. Hydrogen bonding and molecular docking with centromere associated protein inhibitor protein targets summarized in Table-13.

**Drug likeness:** The structural features of the ligand investigated under drug-likeness can predict the efficacy, functionality and fitness of a drug. TPSA, GI absorption and BBB permeability are among the main features researched and calculations are conducted using Lipinski's, Veber's and Ghose filters.

Important ADME parameters like hydrogen bond donor and acceptors (HBD and HBA), molar refractivity (MR), log  $k_p$  (skin permeability) and bioavailability score are also

TABLE-13  
HYDROGEN BONDING AND MOLECULAR DOCKING WITH CENTROMERE  
ASSOCIATED PROTEIN INHIBITOR PROTEIN TARGETS

Protein (PDB ID)	Number of residues	Bond distance (Å)	Inhibition constant (micromolar)	Binding energy (kcal/mol)	Reference RMSD (Å)
5ZWJ	3	2.273	6603	-5.7	9.289

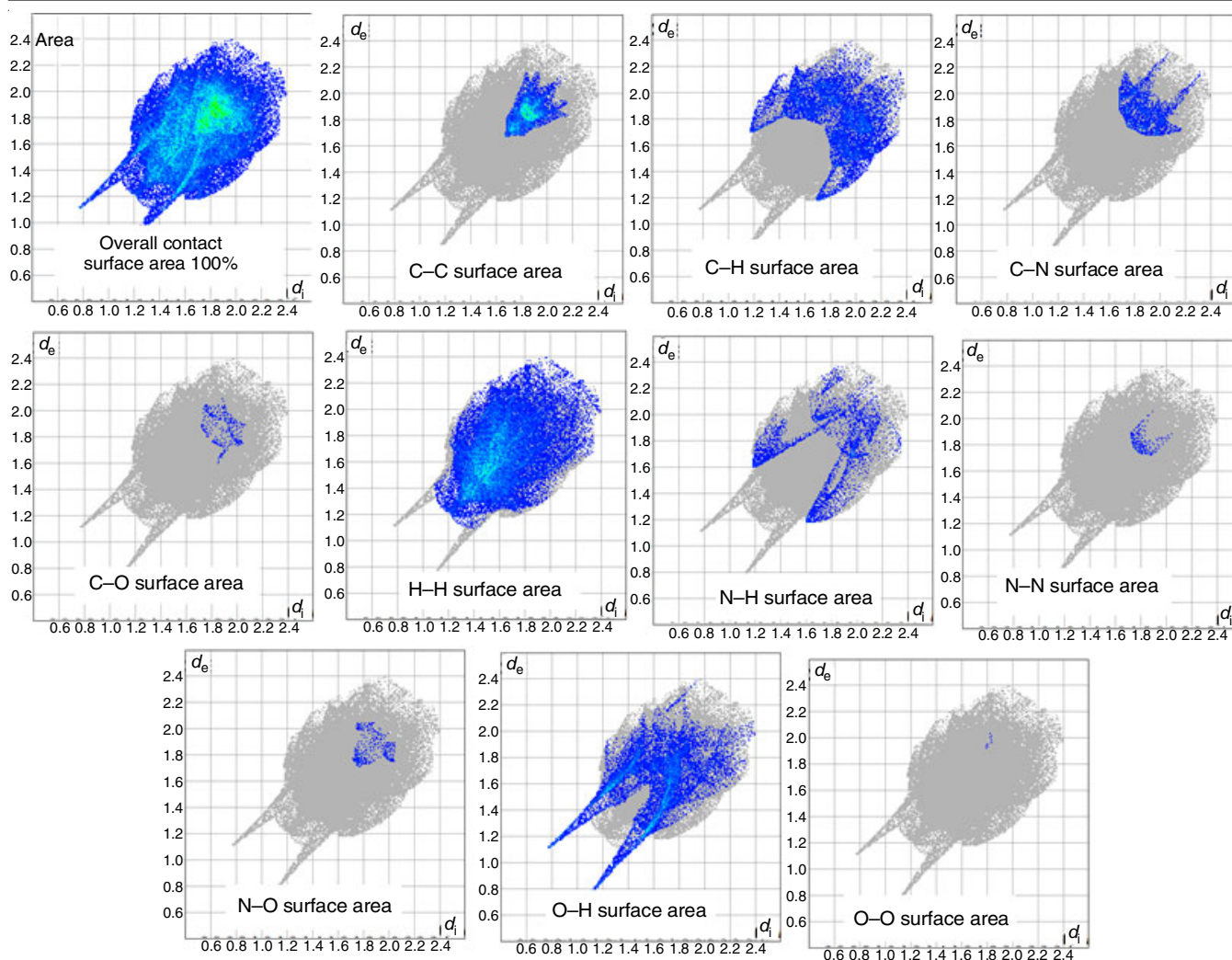


Fig. 11. Fingerprint plots and corresponding surface area of the title compound showing the individual contribution of each interaction

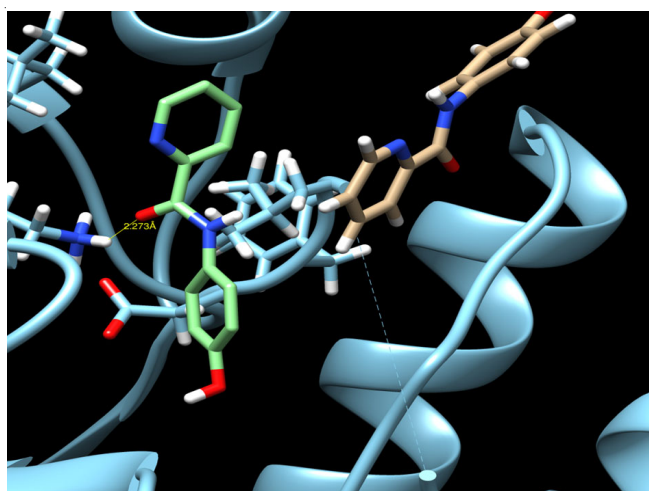


Fig. 12. Ligand 4-HPP embedded in the active site of 5ZWJ protein

calculated and tabulated in Table-14. HBD and HBA values should be less than 10, for this ligand, it is 2. The upper limit for TPSA is  $140 \text{ \AA}^2$  and 4-HPP's value for TPSA is  $62.22 \text{ \AA}^2$ . Molar refractivity is supposed to be between 40 and 130, MR value for MR is 60.47 which is within suggested limits. The molecule has a high GI absorption, it is BBB permeant and its

TABLE-14  
ADME PROPERTIES OF 4-HPP

Properties	4-HPP
HBD	2
HBA	3
MR	60.47
TPSA ( $\text{\AA}^2$ )	62.22
GI Absorption	High
BBB permeant	Yes
CYP1A2 inhibitor	Yes
log Kp (cm/s)	-6.42
Lipinski violations	Yes; 0 violation
Bioavailability score	0.55

skin permeability is  $-6.42 \text{ cm/s}$  with a bioavailability score of 0.55.

Table-14 additionally calculates and tabulates important ADME metrics such as hydrogen bond donor and acceptors (HBD and HBA), molar refractivity (MR), log kp (skin permeability) and bioavailability score. The HBD and HBA values for ligands should be less than 10, whereas the values for 4-HPP it is 2 and 3, respectively. The upper limit of TPSA is  $140 \text{ \AA}^2$ , while the TPSA value of 4-HPP is  $62.22 \text{ \AA}^2$ . The molar refractivity should be between 40 and 130 and for the titled compound, the MR value is 60.47, which is within the recommended

range. The molecule has a high GI absorption rate, is BBB permeant and has a high level of skin permeability.

## Conclusion

The compound, *N*-(4-hydroxyphenyl)picolinamide (4-HPP) was quantum computationally calculated using the B3LYP method and the 6311++G(d,p) basis set and geometry optimization were achieved. All subsequent calculations and analyses were based on this optimized geometry. The RMSD measurements revealed that both structures were similar. The experimental and DFT computed vibrational and NMR data were compared and found to be quite compatible. The interaction energy of electron donation between LP(1)N7→ $\pi^*$ (C3–O8), which gives maximum stabilization energy of 74.82 kJ/mol, is connected to the molecule's resonance. The polarizability values of the compound confirmed that it was an NLO organic molecule. The energy gap between HOMO and LUMO of 3.8766 eV indicated that the molecule is active and stable. FMO studies revealed a lot about compounds in terms of their toxicity and biological activity. Reactive areas were well shown in 3D using MEP, with electrophilic attack vulnerability at O8 and nucleophilic attack vulnerability around H26. The molecule's binding energy with the 5ZWJ protein was -5.7 kcal/mol, indicating that it is non-toxic and drug-likeness.

## ACKNOWLEDGEMENTS

The authors acknowledge Dr. B. R. Ambedkar University, Agra, India for providing necessary computational facilities.

## REFERENCES

- J. Wu, J. Wang, D. Hu, M. He, L. Jin and B. Song, Synthesis and Antifungal Activity of Novel Pyrazolecarboxamide Derivatives Containing a Hydrazone Moiety, *Chem. Cent. J.*, **6**, 51 (2012); <https://doi.org/10.1186/1752-153X-6-51>
- C.-X. Tan, J.-Q. Weng, Z.-X. Liu, X.-H. Liu and W.-G. Zhao, Synthesis, Crystal Structure, and Fungicidal Activity of a Novel 1,2,3-Thiadiazole Compound, *Phosphorus Sulfur Silicon Rel. Elem.*, **187**, 990 (2012); <https://doi.org/10.1080/10426507.2012.664219>
- S. Mahesh, K.-C. Tang and M. Raj, Amide Bond Activation of Biological Molecules, *Molecules*, **23**, 2615 (2018); <https://doi.org/10.3390/molecules23102615>
- N.N. Su, Y. Li, S.J. Yu, X. Zhang, X.H. Liu, W.G. Zhao, N.-N. Su, Y. Li, S.-J. Yu, X. Zhang, X.-H. Liu and W.-G. Zhao, Microwave-Assisted Synthesis of Some Novel 1,2,3-Triazoles By Click Chemistry, and their Biological Activity, *Res. Chem. Intermed.*, **39**, 759 (2013); <https://doi.org/10.1007/s11164-012-0595-9>
- D. Kaiser, A. Bauer, M. Lemmerer and N. Maulide, Amide Activation: An Emerging Tool for Chemoselective Synthesis, *Chem. Soc. Rev.*, **47**, 7899 (2018); <https://doi.org/10.1039/C8CS00335A>
- X. H. Liu, L. Pan, Y. Ma, J. Q. Weng, C. X. Tan, Y. H. Li, Y. X. Shi, B. J. Li, Z. M. Li and Y.G. Zhang, Design, Synthesis, Biological Activities, and 3D-QSAR of New *N,N'*-Diacylhydrazines Containing 2-(2,4-dichlorophenoxy)propane Moiety, *Chem. Biol. Drug Des.*, **78**, 689 (2011); <https://doi.org/10.1111/j.1747-0285.2011.01205.x>
- Y.L. Xue, Y.G. Zhang and X.H. Liu, Synthesis, Crystal Structure, and Biological Activity of 1-Cyano-*N*-(4-bromophenyl)cyclopropanecarboxamide, *Asian J. Chem.*, **24**, 3016 (2012).
- Y.L. Xue, X.H. Liu and Y.G. Zhang, Synthesis, Crystal Structure and Biological Activity of 1-Cyano-*N*-phenylcyclopropanecarboxamide, *Asian J. Chem.*, **24**, 1571 (2012).
- J. Wu, S. Yang, B.-A. Song, P.S. Bhadury, D.-Y. Hu, S. Zeng and H.-P. Xie, Synthesis and Insecticidal Activities of Novel Neonicotinoid Analogs Bearing an Amide Moiety, *J. Heterocycl. Chem.*, **48**, 901 (2011); <https://doi.org/10.1002/jhet.663>
- Y. Xiao, X. Yang, B. Li, H. Yuan, S. Wan, Y. Xu and Z. Qin, Design, Synthesis and Antifungal/Insecticidal Evaluation of Novel Cinnamide Derivatives, *Molecules*, **16**, 8945 (2011); <https://doi.org/10.3390/molecules16118945>
- B.I. Karolyi, S. Bosze, E. Orban, P. Sohar, L. Drahos, E. Gal and A. Csampai, Acylated mono-, bis- and tris- Cinchona-Based Amines Containing Ferrocene or Organic Residues: Synthesis, Structure and *in vitro* Antitumor Activity on Selected Human Cancer Cell Lines, *Molecules*, **17**, 2316 (2012); <https://doi.org/10.3390/molecules17032316>
- B.S. Chhikara, N. St. Jean, D. Mandal, A. Kumar and K. Parang, Fatty Acyl Amide Derivatives of Doxorubicin: Synthesis and *in vitro* Anticancer Activities, *Eur. J. Med. Chem.*, **46**, 2037 (2011); <https://doi.org/10.1016/j.ejmech.2011.02.056>
- J. Wu, S. Kang, B. Song, D. Hu, M. He, L. Jin and S. Yang, Synthesis and Antibacterial Activity Against *Ralstonia Solanacearum* for Novel Hydrazone Derivatives Containing a Pyridine Moiety, *Chem. Cent. J.*, **6**, 28 (2012); <https://doi.org/10.1186/1752-153X-6-28>
- N.C. Singha and D.N. Sathyanarayana, <sup>1</sup>H and <sup>13</sup>C NMR Investigations of *N,N'*-bis(2- and 3-Pyridinyl)-2,6-pyridine Dicarboxamides, *J. Mol. Struct.*, **403**, 123 (1997); [https://doi.org/10.1016/S0022-2860\(96\)09409-4](https://doi.org/10.1016/S0022-2860(96)09409-4)
- R. Wu, C. Zhu, X.-J. Du, L.-X. Xiong, S.-J. Yu, X.-H. Liu, Z.-M. Li and W.-G. Zhao, Synthesis, Crystal Structure and Larvicidal Activity of Novel Diamide Derivatives against *Culex pipiens*, *Chem. Cent. J.*, **6**, 99 (2012); <https://doi.org/10.1186/1752-153X-6-99>
- N.K. Kaushik, A. Mishra, A. Ali, J.S. Adhikari, A.K. Verma and R. Gupta, Synthesis, Characterization, and Antibacterial and Anticancer Screening of {M<sup>2+</sup>-Co<sup>3+</sup>-M<sup>2+</sup>} and {Co<sup>3+</sup>-M<sup>2+</sup>} (M is Zn, Cd, Hg) Heterometallic Complexes, *J. Biol. Inorg. Chem.*, **17**, 1217 (2012); <https://doi.org/10.1007/s00775-012-0937-5>
- A.P. Singh, N.K. Kaushik, A.K. Verma, G. Hundal and R. Gupta, Synthesis, Structure and Biological Activity of Copper(II) Complexes of 4-(2-Pyridylmethyl)-1,7-dimethyl-1,4,7-triazonane-2,6-dione and 4-(2-Pyridylethyl)-1,7-dimethyl-1,4,7-triazonane-2,6-dione, *Eur. J. Med. Chem.*, **44**, 1607 (2009); <https://doi.org/10.1016/j.ejmech.2008.07.029>
- A. Mishra, N.K. Kaushik, A.K. Verma and R. Gupta, Synthesis, Characterization and Antibacterial Activity of Cobalt(III) Complexes with Pyridine-Amide Ligands, *Eur. J. Med. Chem.*, **43**, 2189 (2008); <https://doi.org/10.1016/j.ejmech.2007.08.015>
- A.P. Singh, N.K. Kaushik, A.K. Verma and R. Gupta, Synthesis, Structure and Anticancer Activity of Copper(II) Complexes of *N*-Benzyl-2-(diethylamino)acetamide and 2-(Diethylamino)-*N*-phenylethylacetamide, *Indian J. Chem.*, **50A**, 474 (2011).
- M.V. Solovskij, V.M. Denisov, E.F. Panarin, N.A. Petukhova and A.V. Purkina, Synthesis of Water-soluble Biologically Active Phenol (or Catechol) containing Copolymers of *N*-Vinyl-2-pyrrolidone, *Macromol. Chem. Phys.*, **197**, 2035 (1996); <https://doi.org/10.1002/macp.1996.021970620>
- C.M. Suter and T.B. Johnson, Synthesis of Thiazoles Containing Phenol and Catechol Groups. II, *J. Am. Chem. Soc.*, **52**, 1585 (1930); <https://doi.org/10.1021/ja01367a046>
- A. Ali, G. Hundal and R. Gupta, Co<sup>3+</sup>-Based Building Blocks with Appended Phenol and Catechol Groups: Examples of Placing Hydrogen Bond Donors and Acceptors in a Single Molecule, *Cryst. Growth Des.*, **12**, 1308 (2012); <https://doi.org/10.1021/cg201369g>
- G. Kumar, H. Aggarwal and R. Gupta, Cobalt Complexes Appended with *para*- and *meta*-Arylcarboxylic Acids: Influence of Cation, Solvent, and Symmetry on Hydrogen-Bonded Assemblies, *Cryst. Growth Des.*, **13**, 74 (2013); <https://doi.org/10.1021/cg3011629>
- R.J. Sarma and J.B. Baruah, Supramolecular and Host-Guest Chemistry of Bis-phenol and Analogues, *Cryst. Growth Des.*, **7**, 989 (2007); <https://doi.org/10.1021/cg060899h>

25. C.P. Brock and L.L. Duncan, Anomalous Space-Group Frequencies for Monoalcohols C<sub>n</sub>H<sub>m</sub>OH, *Chem. Mater.*, **6**, 1307 (1994); <https://doi.org/10.1021/cm00044a030>
26. K. Kobayashi, K. Endo, Y. Aoyama and H. Masuda, Hydrogen-Bonded Network Formation in Organic Crystals as Effected by Perpendicular and Divergent Hydroxyl Groups: The Crystal Structure of a Bisresorcinol Derivative of Anthracene, *Tetrahedron Lett.*, **34**, 7929 (1993); [https://doi.org/10.1016/S0040-4039\(00\)61514-9](https://doi.org/10.1016/S0040-4039(00)61514-9)
27. Y. Aoyama, K. Endo, K. Kobayashi and H. Masuda, Hydrogen-Bonded Network and Enforced Supramolecular Cavities in Molecular Crystals: an Orthogonal Aromatic-Triad Strategy. Guest Binding, Molecular Recognition and Molecular Alignment Properties of a Bisresorcinol Derivative of Anthracene in the Crystalline State, *Supramol. Chem.*, **4**, 229 (1994); <https://doi.org/10.1080/10610279408029475>
28. K. Yoshizawa, S. Toyota, F. Toda, M. Kato and I. Csöreg, A New Organic Zeolite Created by Molecular Aggregation of 1,1-bis(3,4-Dihydroxyphenyl)cyclohexane in the Solid State, *CrystEngComm*, **9**, 786 (2007); <https://doi.org/10.1039/b705163h>
29. M. Tominaga, K. Katagiri and I. Azumaya, Pseudopolymorph and Charge-Transfer Co-Crystal of Disubstituted Adamantane containing Dimethoxyphenol Moieties, *Cryst. Growth Des.*, **9**, 3692 (2009); <https://doi.org/10.1021/cg900404h>
30. M. Tominaga, K. Katagiri and I. Azumaya, Hydrogen-Bonded Networks Formed from Tri- and Tetra-substituted Adamantanes bearing Dimethoxyphenol Moieties and their 1,3,5-Trinitrobenzene Complexes via Charge-Transfer Interactions, *CrystEngComm*, **12**, 1164 (2010); <https://doi.org/10.1039/B917654C>
31. M. Tominaga, H. Masu and I. Azumaya, Hydrogen-Bonding Networks of Adamantane-Based Bisphenol Molecules: Toward the Preparation of Molecular Crystals with Channels, *Cryst. Growth Des.*, **11**, 542 (2011); <https://doi.org/10.1021/cg101427k>
32. N. Siddiqui and S. Javed, Quantum Computational, Spectroscopic Investigations on Ampyra (4-Aminopyridine) by DFT/td-dft with Different Solvents and Molecular Docking Studies, *J. Mol. Struct.*, **1224**, 129021 (2021); <https://doi.org/10.1016/j.molstruc.2020.129021>
33. A. Ali, D. Bansal, N.K. Kaushik, N. Kaushik, E.H. Choi and R. Gupta, Syntheses, Characterization and Anticancer Activities of Pyridine-amide Based Compounds Containing Appended Phenol or Catechol Groups, *J. Chem. Sci.*, **126**, 1091 (2014); <https://doi.org/10.1007/s12039-014-0671-3>
34. M.J. Frisch, G.W. Trucks, H.B. Schlegel, G.E. Scuseria, M.A. Robb, R. Cheeseman, J. Montgomer, T. Vreven, K.N. Kudin, J.C. Burant, J.M. Millam, S.S. Iyengar, J. Tomasi, V. Barone, B. Mennucci, M. Cossi, G. Scalmani, N. Rega, G.A. Petersson, H. Nakatsuji, M. Hada, M. Ehara, K. Toyota, R. Fukuda, J. Hasegawa, M. Ishida, T. Nakajima, Y. Honda, O. Kitao, H. Nakai, M. Klene, X. Li, J.E. Knox, H.P. Hratchian, J.B. Cross, V. Bakken, C. Adamo, J. Jaramillo, R. Gomperts, R.E. Stratmann, O. Yazyev, A.J. Austin, R. Cammi, C. Pomelli, J.W. Ochterski, P.Y. Ayala, K. Morokuma, G.A. Voth, P. Salvador, J.J. Dannenberg, V.G. Zakrzewski, S. Dapprich, A.D. Daniels, M.C. Strain, O. Farkas, D.K. Malick, A.D. Rabuck, K. Raghavachari, J.B. Foresman, J.V. Ortiz, Q. Cui, A.G. Baboul, S. Clifford, J. Cioslowski, B.B. Stefanov, G. Liu, A. Liashenko, P. Piskorz, I. Komaromi, R.L. Martin, D.J. Fox, T. Keith, M.A. Al-Laham, C.Y. Peng, A. Nanayakkara, M. Challacombe, P.M.W. Gill, B. Johnson, W. Chen, C. Gonzalez, M.W. Wong and J.A. Pople, Gaussian 03, Revision C. 02, Gaussian Inc., Wallingford, CT, 2004.
35. F. Neese, The ORCA Program System, *WIREs Comput. Mol. Sci.*, **2**, 73 (2012); <https://doi.org/10.1002/wcms.81>
36. M.H. Jomroz, Vibrational Energy Distribution Analysis, VEDA4, Warsaw (2004).
37. T. Lu and F. Chen, Multiwfn: A Multifunctional Wavefunction Analyzer, *J. Comput. Chem.*, **33**, 580 (2012); <https://doi.org/10.1002/jcc.22885>
38. E.F. Pettersen, T.D. Goddard, C.C. Huang, D.M. Greenblatt, G.S. Couch, E.C. Meng and T.E. Ferrin, UCSF Chimera—A Visualization System for Exploratory Research and Analysis, *J. Comput. Chem.*, **25**, 1605 (2004); <https://doi.org/10.1002/jcc.20084>
39. G.M. Morris, R. Huey, W. Lindstrom, M.F. Sanner, R.K. Belew, D.S. Goodsell and A.J. Olson, AutoDock4 and AutoDockTools4: Automated Docking with Selective Receptor Flexibility, *J. Comput. Chem.*, **30**, 2785 (2009); <https://doi.org/10.1002/jcc.21256>
40. A. Daina, O. Michielin and V. Zoete, SwissADME: A Free Web Tool to Evaluate Pharmacokinetics, Drug-likeness and Medicinal Chemistry Friendliness of Small Molecules, *Sci. Rep.*, **7**, 42717 (2017); <https://doi.org/10.1038/srep42717>
41. D.A. Safin, K. Robeyns and Y. Garcia, 1,2,4-Triazole-based Molecular Switches: Crystal Structures, Hirshfeld Surface Analysis and Optical Properties, *CrystEngComm*, **18**, 7284 (2016); <https://doi.org/10.1039/C6CE00749J>
42. G. Socrates, Infrared and Raman Characteristic Group Frequencies, Table and Charts, Wiley: Chichester, Eds. 3 (2001).
43. J. Marshal, FT-Raman and FT-IR Spectra of a Fluoroquinolone Complex, *Indian J. Phys. B*, **72B**, 661 (1998).
44. E.T.G. Lutz and J.H.V. Maas, Structural Information from OH-Stretching Vibrations—XVI. On the Intra- and Intermolecular Interactions of Saturated Tertiary Alcohols in CCl<sub>4</sub> and CS<sub>2</sub>, *Spectrochim. Acta A Mol. Spectrosc.*, **41**, 943 (1985); [https://doi.org/10.1016/0584-8539\(85\)80228-2](https://doi.org/10.1016/0584-8539(85)80228-2)
45. B. Edwin and I. Hubert Joe, Vibrational Spectral Analysis of Anti-neurodegenerative Drug Levodopa: A DFT Study, *J. Mol. Struct.*, **1034**, 119 (2013); <https://doi.org/10.1016/j.molstruc.2012.09.004>
46. L.J. Bellamy, The Infrared Spectra of a Complex Molecule, Wiley: New York, Eds. 3 (1975).
47. S. Pinchas, D. Samuel and M. Weiss-Brodsky, The Infrared Absorption of <sup>18</sup>O-labelled Benzamide, *J. Chem. Soc.*, 1688 (1961); <https://doi.org/10.1039/jr9610001688>
48. G. Varsanyi, Vibrational Spectra of Seven Hundred Benzene Derivatives, Academic Press: New York (1969).
49. H. Sekino and R.J. Bartlett, Hyperpolarizabilities of the Hydrogen Fluoride Molecule: A Discrepancy between Theory and Experiment?, *J. Chem. Phys.*, **84**, 2726 (1986); <https://doi.org/10.1063/1.450348>
50. J. Henriksso, T. Saue and P. Norman, Quadratic Response Functions in the Relativistic Four-component Kohn-Sham Approximation, *J. Chem. Phys.*, **128**, 024105 (2008); <https://doi.org/10.1063/1.2816709>
51. J.P. Hermann, D. Ricard and J. Ducuing, Optical Nonlinearities in Conjugated Systems:  $\beta$ -Carotene, *Appl. Phys. Lett.*, **23**, 178 (1973); <https://doi.org/10.1063/1.1654850>
52. S. Debrus, H. Ratajczak, J. Venturini, N. Pincon, J. Baran, J. Barycki, T. Glowiak and A. Pietraszko, Novel Nonlinear Optical Crystals of Noncentrosymmetric Structure Based on Hydrogen Bonds Interactions Between Organic and Inorganic Molecules, *Synth. Met.*, **127**, 99 (2002); [https://doi.org/10.1016/S0379-6779\(01\)00607-5](https://doi.org/10.1016/S0379-6779(01)00607-5)
53. C.S. Abraham, J.C. Prasana and S. Muthu, Quantum Mechanical, Spectroscopic and Docking Studies of 2-Amino-3-bromo-5-nitropyridine by Density Functional Method, *Spectrochim. Acta A Mol. Biomol. Spectrosc.*, **181**, 153 (2017); <https://doi.org/10.1016/j.saa.2017.03.045>
54. F. Weinhold and L.C. Randis, Valency and Bonding: A Natural Bond Orbital Donor-Acceptor Perspective, Cambridge University Press (2005).
55. P. Rajesh, P. Kandan, S. Sathish, A. Manikandan, S. Gunasekaran, T. Gnanasambandan and S.B. Abirami, Vibrational Spectroscopic, UV-Vis, Molecular Structure and NBO Analysis of Rabeprazole, *J. Mol. Struct.*, **1137**, 277 (2017); <https://doi.org/10.1016/j.molstruc.2017.01.072>
56. J. Liu, Z. Chen and S. Yuan, Study on the Prediction of Visible Absorption Maxima of Azobenzene Compounds, *J. Zhejiang Univ. Sci. B*, **6**, 584 (2005); <https://doi.org/10.1631/jzus.2005.B0584>
57. J.E. Carpenter, J.A. Bohmann, C.M. Morales and F. Weinhold, NBO 5.0, Theoretical Chemistry Institute, University of Wisconsin, Madison, (2001).
58. K. Fukui, Role of Frontier Orbitals in Chemical Reactions, *Science*, **218**, 747 (1982); <https://doi.org/10.1126/science.218.4574.747>

59. S. Balachandar and M. Dhandapani, Biological Action of Molecular Adduct Pyrazole: Trichloroacetic Acid on *Candida albicans* and ctDNA - A Combined Experimental, Fukui Functions Calculation and Molecular Docking Analysis, *J. Mol. Struct.*, **1184**, 129 (2019); <https://doi.org/10.1016/j.molstruc.2019.02.006>
60. C.-G. Zhan, J.A. Nichols and D.A. Dixon, Ionization Potential, Electron Affinity, Electronegativity, Hardness, and Electron Excitation Energy: Molecular Properties from Density Functional Theory Orbital Energies, *J. Phys. Chem. A*, **107**, 4184 (2003); <https://doi.org/10.1021/jp0225774>
61. N.M. O'boyle, A.L. Tenderholt and K.M. Langner, cclib: A Library for Package-independent Computational Chemistry Algorithms, *J. Comput. Inside Chem.*, **29**, 839 (2008); <https://doi.org/10.1002/jcc.20823>
62. H. Tandon, *J. Bioequivalence Bioavailab.*, **9**, 528 (2017);
63. R. Parthasarathi, V. Subramanian, D.R. Roy and P.K. Chattaraj, Electrophilicity Index as a Possible Descriptor of Biological Activity, *Bioorg. Med. Chem.*, **12**, 5533 (2004); <https://doi.org/10.1016/j.bmc.2004.08.013>
64. D.R. Roy, R. Parthasarathi, B. Maiti, V. Subramanian and P.K. Chattaraj, Electrophilicity as a Possible Descriptor for Toxicity Prediction, *Bioorg. Med. Chem.*, **13**, 3405 (2005); <https://doi.org/10.1016/j.bmc.2005.03.011>
65. J.B. Ott and J.B. Goates, *Chemical Thermodynamics: Principles and Applications*, Academic Press, San Diego (2000).
66. F.L. Hirshfeld, Bonded-Atom Fragments for Describing Molecular Charge Densities, *Theor. Chim. Acta*, **44**, 129 (1977); <https://doi.org/10.1007/BF00549096>
67. M.A. Spackman and D. Jayatilaka, Hirshfeld Surface Analysis, *CrystEngComm*, **11**, 19 (2009); <https://doi.org/10.1039/B818330A>
68. W. Wang, Y. Ling, L.-J. Yang, Q.-L. Liu, Y.-H. Luo and B.-W. Sun, Crystals of 4-(2-Benzimidazole)-1,2,4-triazole and its Hydrate: Preparations, Crystal Structure and Hirshfeld Surfaces Analysis, *Res. Chem. Intermed.*, **42**, 3157 (2016); <https://doi.org/10.1007/s11164-015-2203-2>
69. A. Fatima, K. Pooja, S. Savita, M. Singh, I. Verma, N. Siddiqui and S. Javed, Quantum Chemical, Experimental Spectroscopic, Hirshfeld Surface and Molecular Docking Studies of the Antimicrobial Drug Sulfathiazole, *J. Mol. Struct.*, **1245**, 131118 (2021); <https://doi.org/10.1016/j.molstruc.2021.131118>